



Disc regeneration by injectable fucoidan-methacrylated dextran hydrogels through mechanical transduction and macrophage immunomodulation

Weifeng Li^{1,2,4*}, Pinghui Zhou^{1,2*} , Bomin Yan^{1,2*},
Meiyao Qi^{1,2}, Yedan Chen¹, Lijun Shang³, Jianzhong Guan^{1,2},
Li Zhang^{1,2} and Yingji Mao^{1,2,3} 

Abstract

Modulating a favorable inflammatory microenvironment that facilitates the recovery of degenerated discs is a key strategy in the treatment of intervertebral disc (IVD) degeneration (IDD). More interestingly, well-mechanized tissue-engineered scaffolds have been proven in recent years to be capable of sensing mechanical transduction to enhance the proliferation and activation of nucleus pulposus cells (NPC) and have demonstrated an increased potential in the treatment and recovery of degenerative discs. Additionally, existing surgical procedures may not be suitable for IDD treatment, warranting the requirement of new regenerative therapies for the restoration of disc structure and function. In this study, a light-sensitive injectable polysaccharide composite hydrogel with excellent mechanical properties was prepared using dextrose methacrylate (DexMA) and fucoidan with inflammation-modulating properties. Through numerous in vivo experiments, it was shown that the co-culture of this composite hydrogel with interleukin-1 β -stimulated NPCs was able to promote cell proliferation whilst preventing inflammation. Additionally, activation of the caveolin1-yes-associated protein (CAV1-YAP) mechanotransduction axis promoted extracellular matrix (ECM) metabolism and thus jointly promoted IVD regeneration. After injection into an IDD rat model, the composite hydrogel inhibited the local inflammatory response by inducing macrophage M2 polarization and gradually reducing the ECM degradation. In this study, we propose a fucoidan-DexMA composite hydrogel, which provides an attractive approach for IVD regeneration.

Keywords

Dextran, fucoidan, inflammation, mechanical property, nucleus pulposus cells, intervertebral disc degeneration

Date received: 28 March 2023; accepted: 19 May 2023

¹Department of Orthopaedics and Department of Plastic Surgery, The First Affiliated Hospital of Bengbu Medical College, Bengbu, China

²Anhui Province Key Laboratory of Tissue Transplantation, Bengbu Medical College, Bengbu, China

³School of Life Sciences, Bengbu Medical College, Bengbu, China

⁴Department of Orthopedics, Lixin County People's Hospital, Bozhou, China

*These authors contributed equally to this work.

Corresponding authors:

Jianzhong Guan, Department of Orthopaedics and Department of Plastic Surgery, The First Affiliated Hospital of Bengbu Medical College, No. 287 Changhuai Road, Bengbu 233004, China.
Email: guanjianzhong@bbmc.edu.cn

Li Zhang, Department of Orthopaedics and Department of Plastic Surgery, The First Affiliated Hospital of Bengbu Medical College, No. 287 Changhuai Road, Bengbu 233004, China.
Email: drzhangli65@163.com

Yingji Mao, Anhui Province Key Laboratory of Tissue Transplantation, Bengbu Medical College, 2600 Donghai Road, Bengbu 233030, China.
Email: myj123@bbmc.edu.cn



Introduction

Intervertebral disc (IVD) degeneration (IDD) is closely related to axial spinal and neurogenic extremity pain¹ and is considered to be one of the leading causes of neck and lower back pain. Approximately two-thirds of adults worldwide suffer from neck and lower back pain, whilst this is also one of the top four contributors to a disability, thus creating a significant social burden and economic stress.² With the global aging population leading to the increased risk of degenerative diseases, finding effective ways to combat IDD has become an important challenge to be addressed. Currently, the clinical management of disc degeneration typically involves surgical interventions, including disc replacement, resection, and spinal fusion. However, surgery is currently aimed at providing short-term pain relief without restoring the biomechanical function of the disc, while existing surgical procedures may not be suitable for all patients.² Thus, new regenerative therapies for disc degeneration are urgently needed for the restoration of disc structure and function. Recent studies have shown great promise for tissue engineering therapies of disc degeneration, whilst substituting the disc replacements with tissue-engineered manufactured composites that can potentially restore the structural, biological, and mechanical functions of the disc. Numerous tissue engineering studies have focused on the different characteristics of IDD.³

Among these, cell-inoculated hydrogels and other tissue-engineered scaffolds, such as analogs of the nucleus pulposus (NP) region, have been proven as effective entry points.⁴ In the composition of IVD, the NP is a highly hydrophilic substance that uniformly distributes the fluid phase pressure between adjacent vertebral bodies whilst serving an essential role in the axial loading of the spine.^{5,6} Therefore, early IDD first is manifested as high NP loading, which in turn leads to extracellular matrix (ECM) loss or even loss of function. In parallel, excessive spinal load not only leads to disturbances in the metabolism of the ECM of the disc but also upregulates the expression of pro-inflammatory genes, for example, interleukin (IL)-1 β and IL-6.⁵⁻⁷ During this process, activated immune cells (including macrophages, T cells, B cells, and natural killer cells) infiltrate the IVD, which directly affects not only matrix catabolism and anabolism but also indirectly influences ECM homeostasis by inducing the expression of inflammation-related genes (e.g. chemokines and pro-inflammatory cytokines) in the disc cells. This leads to the worsening of the inflammatory and degenerative state of the disc.⁸ Prolonged inflammatory processes not only interfere with the repairing of damaged tissues but can also cause the accumulation of inflammatory cells within the vicinity of the lesion, alongside the formation of local inflammatory cytokine storms, which ultimately impede tissue repair and exacerbate degeneration.⁹ Therefore, finding suitable and effective tissue engineering materials

to replace the NP structure of the IVD, thus mimicking the axial load of the repaired spine by reversing the highly inflammatory microenvironment in the degenerated region through immunomodulation, is a key potential strategy for restoring the IVD structure and function.

Previous studies have reported that fucoidan has a structure similar to chondroitin sulfate, a major component of NP tissue that promotes NP regeneration and ECM synthesis.¹⁰⁻¹² Additionally, fucoidan is a focal sulfated anionic polysaccharide extracted from the sea, which possesses the same sulfate group composition as the glycosaminoglycan found in the ECM of NP, which also confers good immunomodulatory functions.¹³ This component activates macrophage polarization, inhibits pro-inflammatory M1-type macrophage polarization, and promotes anti-inflammatory M2-type polarization, thus inhibiting the production of pro-inflammatory factors whilst exerting anti-inflammatory effects.^{14,15} However, it also inhibits the production of reactive oxygen species (ROS) and blocks nuclear factor (NF)- κ B-mediated inflammatory signaling pathways to slow down the inflammatory process.¹⁶ Recently, its anti-inflammatory ability has been validated and shown to be effective for the treatment of various musculoskeletal disorders, including rheumatoid arthritis and osteoarthritis (OA).^{12,17} We envision that fucoidan enhances the expression of type II Collagen (Col II) and aggrecan (Agg) in disc degeneration by forming an anti-inflammatory microenvironment.¹⁸ Nevertheless, NP is an avascular tissue, and substance exchange in this region is difficult; therefore, there can be problems reaching it using standard systemic delivery methods, which makes loading onto tissue-engineered scaffolds an undoubtedly better option.

Among the many tissue-engineered scaffolds, hydrogels have similar rheological properties to NP whilst also offering excellent biocompatibility and safety,¹⁹ thus providing acute structural and mechanical support for degenerated discs, and are, therefore, an ideal alternative to NP.^{20,21} To combine both stable biomechanical properties and the suppression of local inflammation of the IVD, we propose here loading fucoidan onto a hydrogel scaffold to mimic the NP structure of the IVD. The dextran hydrogel used is a chain-like natural polymer composed of multiple D-glucose molecules with repetitive structures. It is non-toxic, biocompatible, and degradable and can also improve drug stability, alter drug delivery routes, increase drug absorption, and improve drug bioavailability, among other functions.^{22,23} Additionally, it is often used as a novel drug carrier and is expected to be an ideal hydrogel carrier for fucoidans. We synthesized dextrose methacrylate (DexMA) using the introduced methacrylate (MA) group, which is a photo-sensitive characteristic of dextran hydrogel that has remarkable controllability. This is because the performance of DexMA hydrogel can be precisely controlled by changing the ratio of MA and light curing time to achieve *in situ* cross-linking into the gel at the lesion site.²⁴⁻²⁶

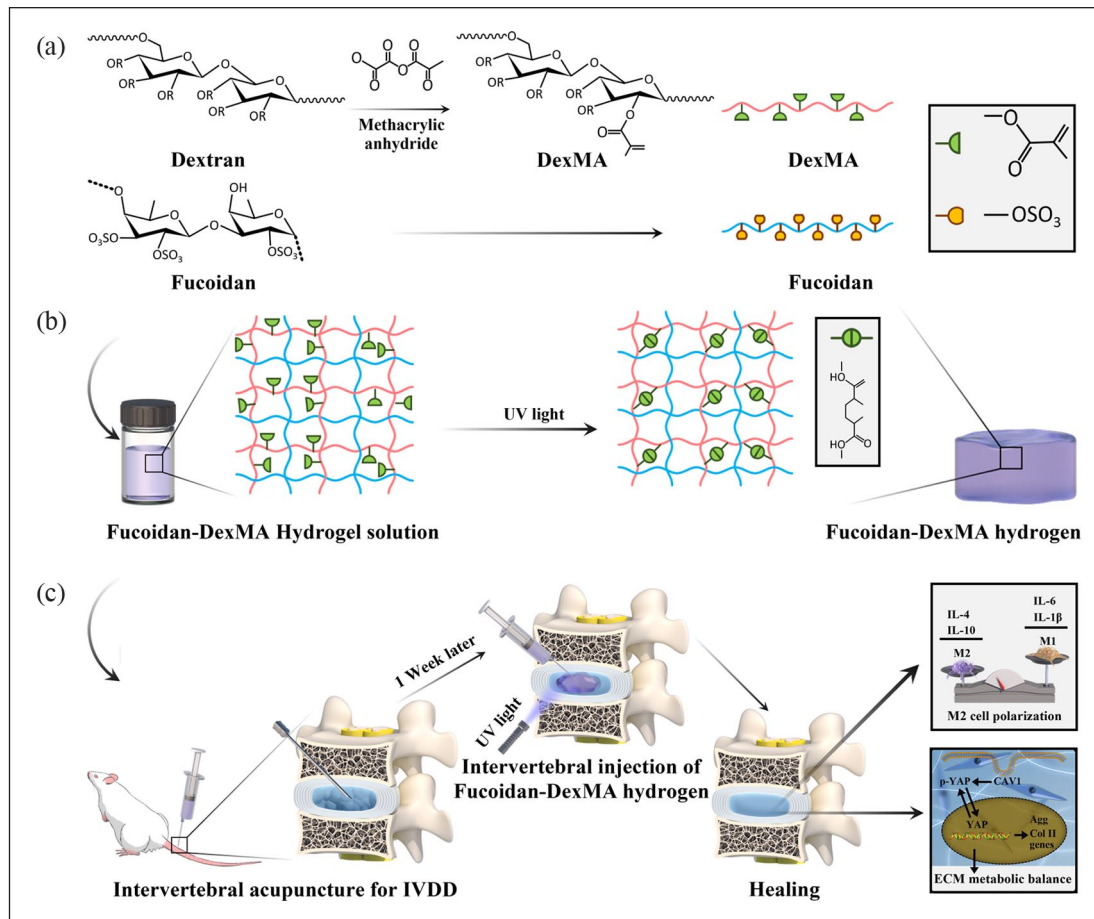


Figure 1. Schematic illustration and fabrication process of fucoidan-DexMA polysaccharide composite hydrogel: (a) synthesis of fucoidan-DexMA hydrogel, (b) fucoidan-DexMA composite hydrogel scaffold fabrication process, and (c) The functions of the fucoidan-DexMA composite hydrogel include promoting M2 polarization, modulating local inflammation, and increasing IVD regeneration.

In summary, by physically mixing fucoidan, which has anti-inflammatory effects, with DexMA hydrogel, an injectable polysaccharide composite hydrogel with mechanically sensitive properties was prepared and its hydrophilic and mechanical properties were subsequently evaluated. *In vitro*, we further evaluated the biocompatibility, anti-inflammatory, and ectoplasmic expression properties of NP cells (NPCs) added to three-dimensional (3D) composite hydrogels treated with IL-1 β . Furthermore, we validated the potential of the fucoidan-DexMA composite hydrogel for improving the inflammatory microenvironment of the NP and repairing disc degeneration in a rat caudal disc degeneration model (Figure 1). The results show fucoidan-DexMA composite hydrogel as a promising disc repair option in protecting NPCs, improving the inflammatory environment, and restoring the biomechanical structure of the IVD to stop the development of IDD.

Materials and methods

Preparation of the composite hydrogel scaffold

DexMA was synthesized by methacrylation of dextran and glycidyl methacrylate (Aladdin, Shanghai, China).^{27,28} In brief, dextran (20 g, 147 kDa) and 4-dimethylaminopyridine (2 g) were dissolved in anhydrous dimethyl sulfoxide (100 ml) and stirred vigorously to obtain a homogeneous mixture. Subsequently, glycidyl methacrylate (24.6 ml) was added whilst vigorously stirring, and the reaction was then maintained by heating at 45°C for 24 h. After cooling on ice for 20 min, the mixture was then precipitated in 1 l of pre-cooled 2-isopropanol to obtain DexMA. The crude product collected by centrifugation was dissolved in double-distilled water (ddH₂O) and dialyzed for 3 days against ddH₂O. After purification by dialysis, DexMA was lyophilized to obtain the final product, which was then stored at -20°C during the following experiments.

The photoinitiator, lithium phenyl-2,4,6-trimethylbenzoylphosphonate (LAP, EFL, Suzhou, China), was weighed and dissolved in phosphate-buffered saline (PBS) at 40–50°C to prepare a 0.25% (w/v) solution. Additionally, a 5% (w/v) DexMA solution was prepared by adding DexMA to the abovementioned solution and stirring. Fucoidan from *Fucus vesiculosus* (Sigma-Aldrich, Shanghai, China) at different concentrations of 0, 1, 2, 4, and 8 mg/ml (w/v) was subsequently added. Finally, the mixture was filtered through a 0.22 µm filter and crosslinked by irradiation with ultraviolet (UV) light (83 mW/cm², 405 nm) for 30 s in the dark to prepare the fucoidan-DexMA composite hydrogel.

Characterization of the composite hydrogel scaffold

Nuclear magnetic resonance (NMR) imaging. Dextran and DexMA were detected by ¹H NMR (Bruker 400M, Falanden, Switzerland), and the analysis was performed using MestReNova software (version 14.0; Mestrelab Research, Spain) to assess whether MA was modified on dextran. The degree of substitution (DS) of DexMA was calculated using the ratio between the average integrated area of the methacrylate protons (6.12 and 5.67 ppm in D₂O) and the anomeric proton of the glycopyranosyl ring (4.87 ppm), as shown by the following formula:

$$DS = \frac{A(\delta 6.12 \& \delta 5.67) / 2}{A(\delta 4.87)} \times 100\%$$

Scanning electron microscope (SEM) analysis. Composite hydrogel scaffolds with a diameter of 1 cm and a thickness of 5 mm were prepared by UV irradiation. These hydrogels were then refrigerated at –20°C for 24 h, followed by lyophilization at –40°C for 18 h (SIM, Los Angeles, USA). The dried samples were then sprayed with gold and observed using an SEM (Zeiss Gemini 300, Oberkochen, Germany). The mean pore sizes of the samples were measured by analyzing five random regions using the ImageJ software (National Institutes of Health, Bethesda, MD, USA).

Water contact angle (WCA) analysis. The hydrophilicity of the hydrogel scaffolds was evaluated by measuring the static WCA and the droplet shape on a scientific surface analyzer (Dataphysics OCA20, Stuttgart, Germany) at 25°C. Each experiment was repeated three times.

Mechanical testing. The compressive moduli of the pure DexMA and fucoidan-DexMA composite hydrogels (a cylinder 8 mm in diameter and 3 mm in height) were measured using a universal electromechanical testing machine (Instron 5944, Norwood, MA, USA). A constant compression rate of 1 mm/min was used, whilst the compressive

modulus of the hydrogel was determined by calculating the slope of the stress-strain curve up to a strain of 20%. Three replicates were used for each group.

Drug release testing. The analysis of fucoidan release capacity in fucoidan-DexMA composite hydrogel was tested according to the method previously described in the literature.¹⁸ The absorbance of residual toluidine blue was measured at 630 nm using a UV-Vis spectrophotometer, which generated a calibration curve and determined the concentration of fucoidan.

In vitro performance

NPC culture. NPCs were extracted from Sprague-Dawley (SD) rats (4 weeks old, 75–95 g) as described in our previous methods²⁹ and cultured in a 37°C incubator with 5% CO₂ using Dulbecco's Modified Eagle's Medium (DMEM)/F12 (Gibco, Shanghai, China) complete medium with 10% fetal bovine serum (Hyclone, Wuhan, China) and 1% penicillin-streptomycin (Biosharp, Hefei, China). The medium was refreshed every 2 days, and the cells were passaged after reaching 70–80% confluency until the third generation and used for subsequent experiments.

NPC encapsulated in hydrogel. NPCs (1 × 10⁶ cells/ml) were uniformly suspended and mixed with DexMA and fucoidan-DexMA solution. Then, the suspension was injected into a circular mold with a diameter of 5 mm and a thickness of 2 mm and crosslinked with UV light to construct the NPC-encapsulated hydrogel. These scaffolds were immediately incubated in DMEM/F12 medium, and the medium was refreshed every 2 days.

Cell viability and proliferation in hydrogel. After 1 and 3 days of incubation, the viability of the NPC-encapsulated hydrogel was assessed using the live/dead staining kit (Beyotime, Shanghai, China). In brief, a mixed solution of calcein-AM and propidium iodide (PI) was added and incubated with hydrogel samples at 37°C in the dark for 30 min. After removing the solution, the cells were visualized and quantified under a laser scanning confocal fluorescence microscope (LSCM, Olympus, Tokyo, Japan), in which living cells were marked with green fluorescence by calcein-AM, whilst dead cells were marked with red fluorescence by PI.

Cell proliferation was determined using a Cell Counting Kit-8 (CCK-8; Biosharp, Hefei, China). NPCs (2 × 10³ cells per well) were encapsulated in the hydrogel and cultured in a 96-well plate after UV light irradiation. At predetermined time points, DMEM/F12 containing 10% CCK-8 solution was added to each well, followed by incubation for 2 h. The optical density (OD) of the supernatant was measured at 450 nm using an enzyme-labeling instrument (BioTek, Vermont, USA). Three replicates were again used for each group.

Cell proliferation can be further explored by EdU incorporation assay. The NPCs were encapsulated in the hydrogel and then stained according to the reagent manufacturer's instructions. Fluorescent microscopy was employed to observe the cells and quantitative analysis of the fluorescence images was performed using ImageJ software.

To examine PCNA (Proliferating Cell Nuclear Antigen) protein expression, the pre-treated NPCs were encapsulated in the composite hydrogel and cultured for 24 h. The DexMA composite hydrogels were soaked in DexMA Lysis Solution (Suzhou, China) for 30 min at room temperature until complete dissolution. The cells were then lysed using radioimmunoprecipitation assay (RIPA) lysis buffer (Beyotime, Shanghai, China). The isolated proteins were separated using 10% sodium dodecyl sulfate-polyacrylamide gel electrophoresis (SDS-PAGE) and transferred to polyvinylidene fluoride (PVDF) membranes (Millipore, Billerica, MA, USA). Subsequently, the membranes were blocked with 5% non-fat milk in Tris-buffered saline (TBS) solution with the detergent Tween® 20 (TBST, 10 mM pH 7.6 Tris-HCl, 100 mM NaCl, and 0.1% Tween 20) for 2 h, then incubated with PCNA antibody (1:3000, ab92552, Abcam) overnight at 4°C. After washed with TBST and then incubated with goat anti-rabbit horseradish peroxidase (HRP)-coupled secondary antibody (1:5,000, S0001, Affinity) at room temperature, PCNA protein expression was examined using a chemiluminescent reagent (Beyotime), and the signal intensity was quantified using ImageJ software.

IL-1 β -induced NPC-encapsulated hydrogel under inflammation condition. To stimulate the inflammatory microenvironment, NPCs were pre-treated and incubated in DEMF/F12 medium with 10 ng/ml IL-1 β (Sino Biological, Beijing, China) for 24 h.³⁰ Subsequently, all the cells were harvested and encapsulated in the hydrogel, as described above. At predetermined time points, the viability of encapsulated NPCs in the hydrogel was evaluated using a live/dead staining kit, as previously mentioned.

Immunofluorescence analysis under inflammation condition. After treatment with 10 ng/ml IL-1 β , NPC-encapsulated hydrogels were cultured for 24 h and fixed with 4% paraformaldehyde for 30 min at room temperature. Subsequently, the samples were embedded in an O.C.T compound (Sakura Finetek, USA) overnight at 4°C, then frozen at -20°C, and eventually sliced into 20- μ m-thick sections using a cryostat (Leica, Weztlar, Germany).

To investigate the effect of the CAV1-YAP-mediated mechanotransduction pathway on NPC-encapsulated hydrogel scaffolds at different levels of stiffness, CAV1 and YAP immunofluorescence staining was performed according to the following protocols. After washing with PBS, sections were permeabilized with 0.3% Triton X-100 at 10°C for 15 min. The sections were then blocked with

1% bovine serum albumin (BSA, Invitrogen, Shanghai, China) for 1.5 h and incubated with primary antibodies: CAV1 (1:500, 16447-1-AP, Proteintech) or YAP (1:100, A1001, ABclonal) at 4°C overnight. Subsequently, the sections were washed with PBS and incubated with either fluorescein isothiocyanate (FITC)-labeled antibody (1:100, AS024, ABclonal) or sulfo-Cyanine3 (Cy3)-labeled antibody (1:400, AS007, ABclonal) for 2 h at room temperature. Finally, the sections were counterstained using 4',6-diamidino-2-phenylindole (DAPI) and mounted with VECTASHIELD (Vector Laboratories, San Francisco, CA, USA). Images were observed and captured using an LSCM. Semi-quantitative fluorescence analysis was conducted using ImageJ software.

To evaluate the expression of ECM-related proteins (Agg and Col II), immunofluorescence staining was performed, as previously described. In brief, the sections were incubated with primary antibodies: Anti-Agg antibody (1:200, DF7561, Affinity) or anti-Col II antibodies (1:200, AF0135, Affinity) at 4°C overnight. The sections were then labeled with either Alexa Fluor 488-labeled antibody (1:200, S0018, Affinity) or Cy3-labeled antibody (1:400, AS007, ABclonal) for 2 h. After staining with DAPI, the images were obtained using an LSCM.

The subcellular distribution of YAP, the ratio of translocated YAP, and fluorescence densities of Col II and Agg were all quantified using ImageJ software, following the previously reported protocols.^{31,32}

Western blot assay under inflammation condition. Western blotting was performed to assess the influence of the CAV1-YAP-mediated mechanotransduction pathway and the anti-inflammatory effects of the NPC-encapsulated composite hydrogel under inflammatory conditions. Proteins were labeled and incubated overnight at 4°C with the following primary antibodies: YAP (1:500, A1001, ABclonal), p-YAP (1:500, AP0489, ABclonal), CAV1 (1:2000, 16447-1-AP, Proteintech), Col II (1:2000, ab188570, Abcam), Agg (1:2000, DF7561, Affinity), IL-1 β (1:1000, AF5103, Affinity), IL-6 (1:1000, DF6087, Affinity), IL-10 (1:1000, DF6894, Affinity), IL-4 (1:1000, AF5142, Affinity), and β -actin (1:5000, AF7018, Affinity). After washing using TBST buffer, the membranes were treated with horseradish peroxidase (HRP)-conjugated secondary antibody (1:5000, S0001, Affinity) for 2 h at room temperature. Then examined with a chemiluminescent reagent (Beyotime), and quantified the signal intensity using ImageJ software.

Enzyme-linked immunosorbent assay (ELISA). To investigate the ability of ECM secretion and the concentration of inflammatory factors in NPC-encapsulated hydrogels, ELISA was conducted according to the manufacturer's protocol. In brief, pre-treated NPCs with IL-1 β were encapsulated in the composite hydrogel and cultured for

24 h. Then, the supernatant was collected, and the concentrations of target proteins (Col II, Agg, IL-1 β , IL-6, IL-4, and IL-10) were measured using an ELISA kit (Dakewe, Shenzhen, China).

In vivo performance

Experimental animals. Seven-week-old male SD rats (200–250 g) were purchased from the Shushan Experimental Animal Center (Hefei, China) and acclimatized to the vivarium for 1 week before the experiments. All procedures and treatments were approved by the Institutional Animal Care and Use Committee of Bengbu Medical College (approval no. 2020139). All rats were housed in a room with a 12 h light/dark cycle and free access to food and water.

Surgical procedure. The puncture-induced IDD rat model was established as previously described.³³ Sixty SD rats were anesthetized intraperitoneally with 1% pentobarbital. Digital palpation was used to locate the caudal disc (Co6/Co7), which was then confirmed using trial radiography. A sterile 21 G needle was used to percutaneously pass through the annulus fibrosus into the middle of the NP. To ensure the degeneration effect, the needle was used at a depth of 5 mm using a stopper, rotated 360°, and then held in this position for 30 s. The rats were randomly divided into five groups ($n=12$ for each group): sham group (not punctured), control group (punctured without injection), fucoidan group (punctured and injected with 4 mg/ml fucoidan), DexMA group (punctured and injected with 5% DexMA hydrogel), and Fuc-Dex group (punctured and injected with 4 mg/ml fucoidan-5% DexMA composite hydrogel). A week after IVD induction, each disc was injected with 20 μ l hydrogel solution using a 31 G microsyringe, followed by irradiation with UV light (83 mW/cm², 405 nm) for 30 s to gel *in situ*. All experiments were carried out under aseptic conditions, and the rats were housed in a warm and ventilated environment. After injection at 4 and 8 weeks, radiography, magnetic resonance imaging (MRI), and histological analysis were performed.

Disc height measurement. Changes in the caudal IVD were measured using a digital X-ray machine (Siemens, Berlin, Germany). All anesthetized rats were placed in the supine position, with their tails kept straight. The average heights of the IVD and adjacent vertebral bodies were measured using ImageJ software, according to previously reported protocols.³⁴ The IVD height indices (DHI; Supplemental Figure S4) were calculated using the following formula:

$$DHI = 2x \frac{DH1 + DH2 + DH3}{(PV1 + PV2 + PV3) + (DV1 + DV2 + DV3)}$$

where PV indicates a proximal vertebral body and DV indicates a distal vertebral body. Changes in IVD height

were described using the percentage of punctured group DHI to sham group DHI and expressed as DHI%.

MRI examination. A 1.5 T MRI scanning system (Philips, Amsterdam, Netherlands) was used to access the sagittal T2-weighted signal images of the IVD structure. The parameters of the MRI scanning system were set as follows: repetition time (TR) 2500 ms, echo time (TE) 30 ms, field of view 200, and slice thickness 2 mm. MRI images were evaluated blindly according to the Pfirrmann MRI grading score (see Table S1). Additionally, the gray values of all pixels in the NP region of the IVDs in the images were calculated using ImageJ software.³⁵

Histological analysis. After euthanasia of rats by overdose anesthetic injection, the coccygeal discs were harvested, fixed in 4% paraformaldehyde for 24 h, and then decalcified in 10% ethylenediaminetetraacetic acid (EDTA) for 4 weeks, and the medium was refreshed daily. The samples were subsequently dehydrated using graded ethanol and embedded in paraffin. The samples were sliced into 5 μ m sagittal sections containing the NP, annulus fibrosus, and end plates. Hematoxylin and eosin (H&E) and safranin O-fast green staining were performed to observe collagen remodeling and deposition. Histological morphology was captured using microscopy, whilst the degenerative degree of the IVD was scored according to the previously described Masuda protocol (Table S2).³⁶ Scores of 4, 5–11, and 12 indicate normal discs, moderately degenerated discs, and severely degenerated discs, respectively.

Immunohistochemistry. To evaluate *in vivo* changes in ECM secretion, levels of inflammatory cytokines, and macrophage polarization, the sections were immunohistochemically stained. Briefly, deparaffinized sections were incubated with 3% H₂O₂ for 15 min in the dark and then blocked with 3% BSA for 30 min at room temperature. The sections were incubated overnight at 4°C along with the following primary antibodies: Col II (1:500, GB111629, Servicebio), aggrecan (1:500, GB11373, Servicebio), IL-1 β (1:200, AF5103, Affinity), IL-6 (1:200, DF6087, Affinity), IL-10 (1:200, DF6894, Affinity), IL-4 (1:200, AF5142, Affinity), CD68 (1:300, GB113109, Servicebio), Arg1 (1:500, GB11285, Servicebio), and CC-chemokine receptor 7 (CCR7) (1:300, GB11502, Servicebio). After primary antibody incubation, the sections were incubated with a specific HRP-conjugated secondary antibody (1:200, S0001, Affinity) for 1 h at 25°C. The sections were stained with 3,3'-diaminobenzidine and counterstained with hematoxylin for the nucleus. Finally, the sections were mounted and photographed using an optical microscope (Nikon, Tokyo, Japan). Immunohistochemical staining intensity was digitally quantified using ImageJ software.

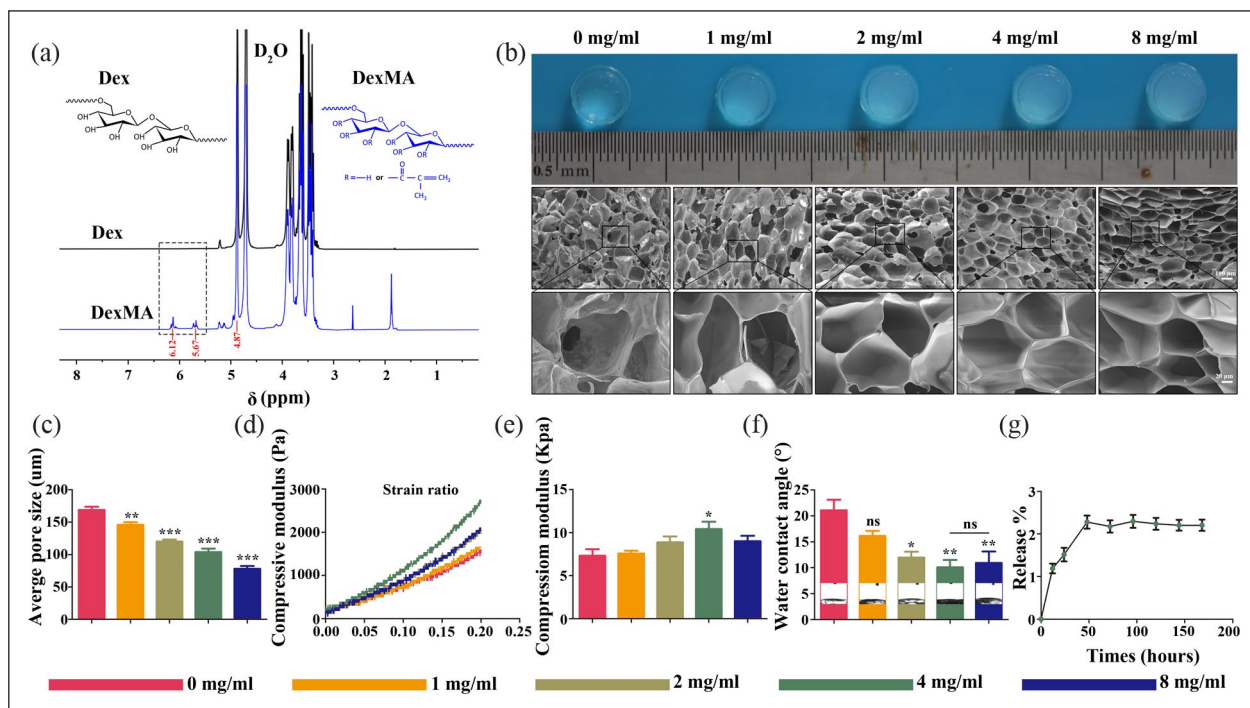


Figure 2. Morphology and characterization of composite scaffolds: (a) ¹H NMR spectra and chemical structures of Dex and DexMA, (b) bright fields and SEM internal pore structure images of the composite scaffolds, (c) quantitative analysis of the pore size (μm) of composite hydrogel scaffold, (d) compressive modulus strain rate and compressive modulus of different composite scaffolds, (e) WCA of different composite hydrogel scaffolds, (f) WCA of different composite hydrogel scaffolds, and (g) the release curves of fucoidan in the hydrogel.

* $p < 0.05$. ** $p < 0.01$. *** $p < 0.001$ versus control group, ns indicates no significant difference).

Statistical analysis

All data are presented as the mean \pm standard deviation (S.D) of at least three independent experiments. One-way analysis of variance (ANOVA) followed by Tukey's tests was used for comparisons between the two groups. The results were analyzed and subsequently compared using GraphPad Prism 5.0 (GraphPad Software, CA, USA). Statistical significance was set at $p < 0.05$ (* $p < 0.05$. ** $p < 0.01$. *** $p < 0.001$. ns = not significant).

Results

Composite hydrogel characterization

In this study, DexMA was synthesized *via* a substitution reaction between the hydroxyl and methacryloyl groups of dextran. Therefore, in the presence of the LAP initiator, the DexMA functional groups could be crosslinked by UV irradiation. To demonstrate successful modification, the synthesized monomer hydrogel was dissolved in D₂O and characterized by ¹H NMR spectroscopy. As shown in Figure 2(a), which compares the spectra of dextran and DexMA, new peaks were observed at δ 6.12 and δ 5.67 ppm. These were assigned to the vinyl protons in DexMA, which was also supported by previous studies.²⁸ The degree of methacrylated dextran was 5.4%, according to the integrated area in the ¹H NMR spectrum.

SEM analysis was performed to identify the microstructures of composite hydrogels mixed with different concentrations of fucoidan. As shown in the SEM micrograph (Figure 2(b)), the cross sections of the composite hydrogel exhibited a classical porous honeycomb structure. The pore size of the honeycomb lattice gradually decreased from 200 to 70 μm as the concentration of fucoidan increased, whilst a higher concentration of fucoidan resulted in a denser gel network structure with a higher porosity (Figure 2(c)).

Generally, the deformation resistance and elasticity of fucoidan-DexMA composite hydrogel scaffolds are associated with the long-term stability of the NP structure. To further identify the effect of fucoidan incorporation on the mechanical strength of the composite hydrogels, we evaluated the mechanical strength of different scaffolds using compressive modulus tests at 20% strain compression (Figure 2(d) and (e)). Interestingly, the compressive modulus of the composite hydrogel scaffold with a concentration of 4 mg/ml was almost 1.5 times higher than that of the control 5% DexMA hydrogel scaffold alone (7.31 ± 1.88 kPa). In contrast, mixing with other concentrations of fucoidan did not significantly affect the mechanical strength of the composite hydrogel. Previous studies have determined the required mechanical strength of natural IVDs (5–35 kPa), whilst it can also be seen that a composite hydrogel scaffold mixed with a concentration of

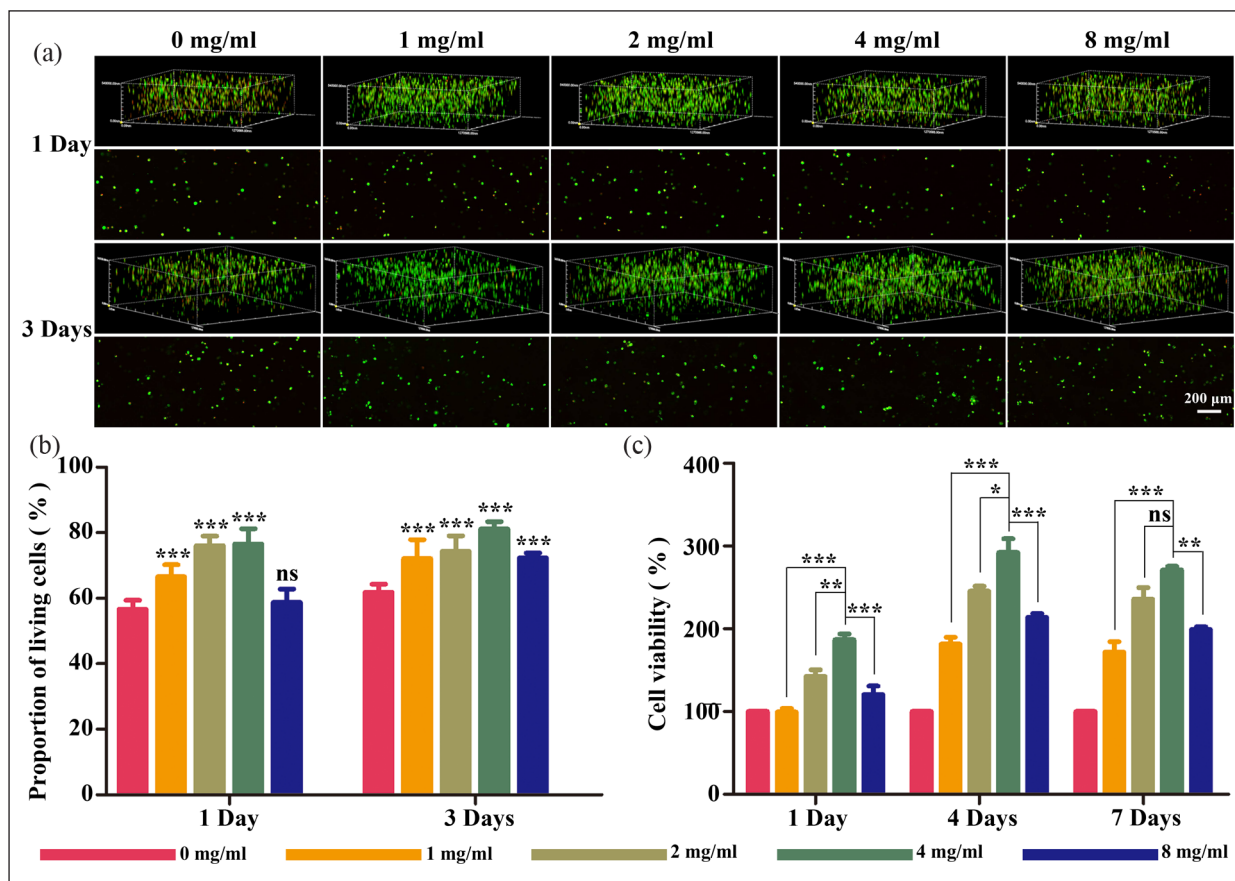


Figure 3. Viability and proliferation of NPCs in fucoidan-DexMA: (a) live/dead staining of NPCs cultured in hydrogel for 1 and 3 days. Green: living cells. Red: dead cells; scale bar, 200 μm, (b) quantitative analysis of live NPCs in the hydrogel scaffold, and (c) the proliferation of NPCs cultured in different materials for 1, 4, and 7 days was assessed using a CCK-8 kit (compared with the control group, * $p < 0.05$. ** $p < 0.01$. *** $p < 0.001$. ns indicates no significant difference).

4 mg/ml fucoidan would be more compatible to maintain the mechanical strength of the natural NP and also more suitable for injection as a replacement material for IVD tissues.

The hydrophilicity of the scaffold is another major characteristic of hydrogel scaffold materials. Materials with high hydrophilicity facilitate the penetration and delivery of nutrients, which can provide a favorable local microenvironment for cell growth. The hydrophilic properties of the hydrogels were evaluated through WCA assay (Figure 2(f)), with the results demonstrating that different concentrations of the composite hydrogels had good hydrophilic properties. Compared with the control group (containing a fucoidan concentration of 0 mg/ml and WCA of $21.09^\circ \pm 3.49^\circ$), the WCA decreased with increasing fucoidan concentrations, which represented the increasing hydrophilicity of the scaffold. Nevertheless, at concentrations >4 mg/ml, the hydrophilicity of the scaffolds no longer increased significantly. This implied that the composite hydrogel scaffold WCA was $10.07^\circ \pm 2.48^\circ$ at a fucoidan concentration of 4 mg/ml, which had the optimal hydrophilic activity.

The release of fucoidan in different groups of hydrogel scaffolds was quantified and results (supplemental Figure S1 and 2G) indicated that in fucoidan-DexMA composite hydrogel, nearly 2% of fucoidan release around the 60th hour and stopping further releasing, the total amount of released fucoidan with 2% release could be maintained in DexMA hydrogel for more than 7 days.

In vitro performance evaluation

Cell viability and proliferation in the hydrogel. To determine the biocompatibility of fucoidan-DexMA, we investigated the survival and proliferation of NPCs in the different hydrogel groups. The viability of cells encapsulated in the different groups was evaluated using live/dead staining. A correlation between the fucoidan amount and cell viability was subsequently observed (Figure 3(a) and (b)). With increasing amounts of fucoidan, cell viability was improved at different time points (1 and 3 days). Interestingly, on the third day, the percentage of living cells in all different material groups increased compared with that on the first day, with the 4 mg/ml group exhibiting the most

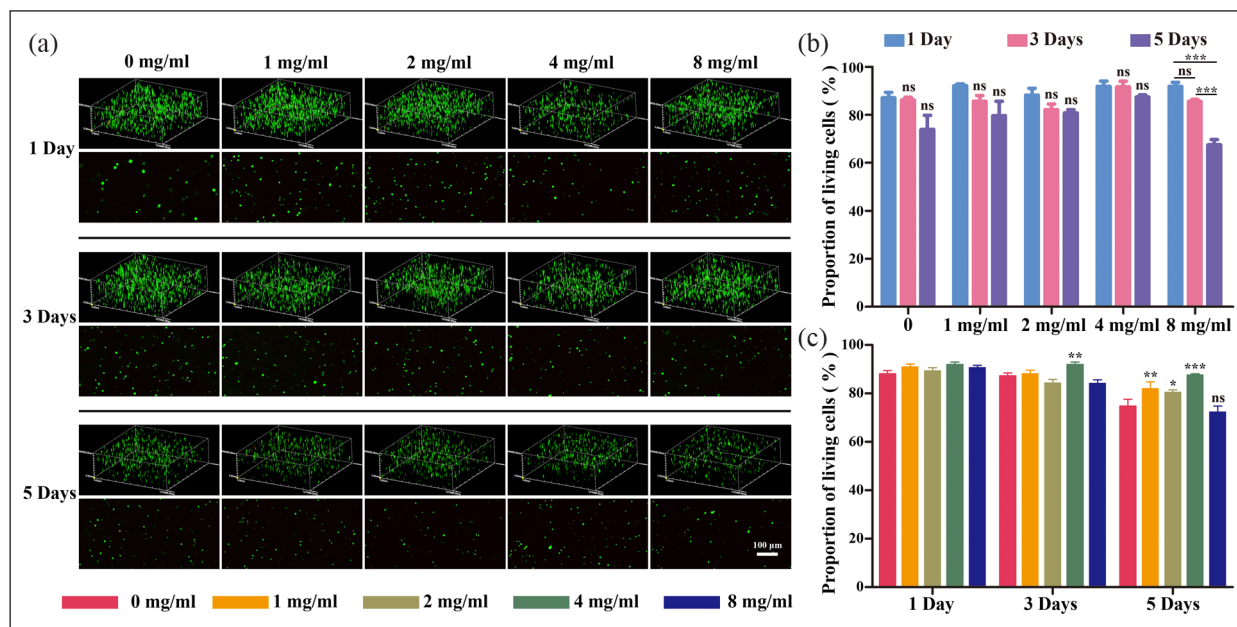


Figure 4. Cell activity of NPCs encapsulated in fucoidan-DexMA cultured in an inflammatory environment (IL-1 β 10 ng/ml) *in vitro*: (a) live/dead staining of encapsulated NPCs cultured in different hydrogel scaffolds for 1, 3, and 5 days. Green: living cells; Red: dead cells; scale bar, 200 μ m, (b and c) quantitative analysis of living cells in fucoidan-DexMA at different time intervals (b) and in different groups (c) (compared with the control group, * p < 0.05. ** p < 0.01. *** p < 0.001, ns indicates no significant difference).

pronounced increase. We assessed the proliferation of NPCs encapsulated in fucoidan-DexMA using a CCK8 assay (Figure 3(c)). Similarly to the live/dead staining results, increasing the concentration of fucoidan significantly enhanced cell proliferation, whilst the 4 mg/ml group exhibited the highest proliferation rate. The Edu assay showed the same trend as the CCK-8 assay (Supplemental Figure S2), and the incorporation of 4 mg/ml of fucoidan allowed the DexMA hydrogel to exhibit optimal biocompatibility. PCNA is an indicator of the proliferation status of cells, and the expression levels of PCNA were analyzed by western blotting (Supplemental Figure S3). The quantitative analysis further indicated that the expression of PCNA in NPC grown on DexMA hydrogel scaffolds with the addition of 4 mg/ml fucoidan far exceeded that of the DexMA hydrogel group without fucoidan on day 1, and maintained its dominance for 1 week. Combining all the above results, it can be concluded that 4 mg/ml is the fucoidan incorporation concentration to maintain the best biocompatibility of the Fucoidan-DexMA scaffold.

Cell viability in an inflammatory environment. IL-1 β is among the most critical pro-inflammatory factors associated with the initiation and progression of degenerative disc disease (DDD), which triggers higher levels of pro-inflammatory mediators (including TNF- α , IL-6, and some matrix-degrading enzymes) that disrupt ECM metabolic homeostasis and impair metabolism. To verify the activity of NPCs in the inflammatory environment during disc degeneration, 10 ng/ml IL-1 β was incorporated into the culture

medium for inflammatory stimulation to mimic the inflammatory environment during disc degeneration, and live/dead staining was performed. The survival of the cells in each group was good, as illustrated by the fluorescence images (Figure 4(a)). After statistical and quantitative analyses, it was clear that overall, no significant differences in the ratio of viable cells were observed between groups on both the first and third days (Figure 4(b)). By the fifth day, there were no significant differences among the groups, except for the 8 mg/ml group, indicating that the survival of NPCs was not significantly affected by fucoidan concentrations below 4 mg/ml. A cross-sectional comparison of the results from each assay (Figure 4(c)) revealed that there were no significant differences in the viable cell ratios among the groups on the first day. Nevertheless, on the third day, a significant increase in the viable cell ratio appeared in the 4 mg/ml group compared with that of the control group, unlike in the other groups, whilst this trend became more pronounced by the fifth day. It can be concluded that there was a correlation between the concentration of fucoidan in the scaffold and the activity of cells in the inflammatory environment, where a loading concentration of 4 mg/ml of fucoidan would significantly contribute to the survival of NPCs in the hydrogel composite scaffold.

***In vitro* anti-inflammatory effect of the composite hydrogel.** Several previous studies have demonstrated that fucoidan attenuates the inflammatory responses in various tissues. To determine the *in vitro* anti-inflammatory effects

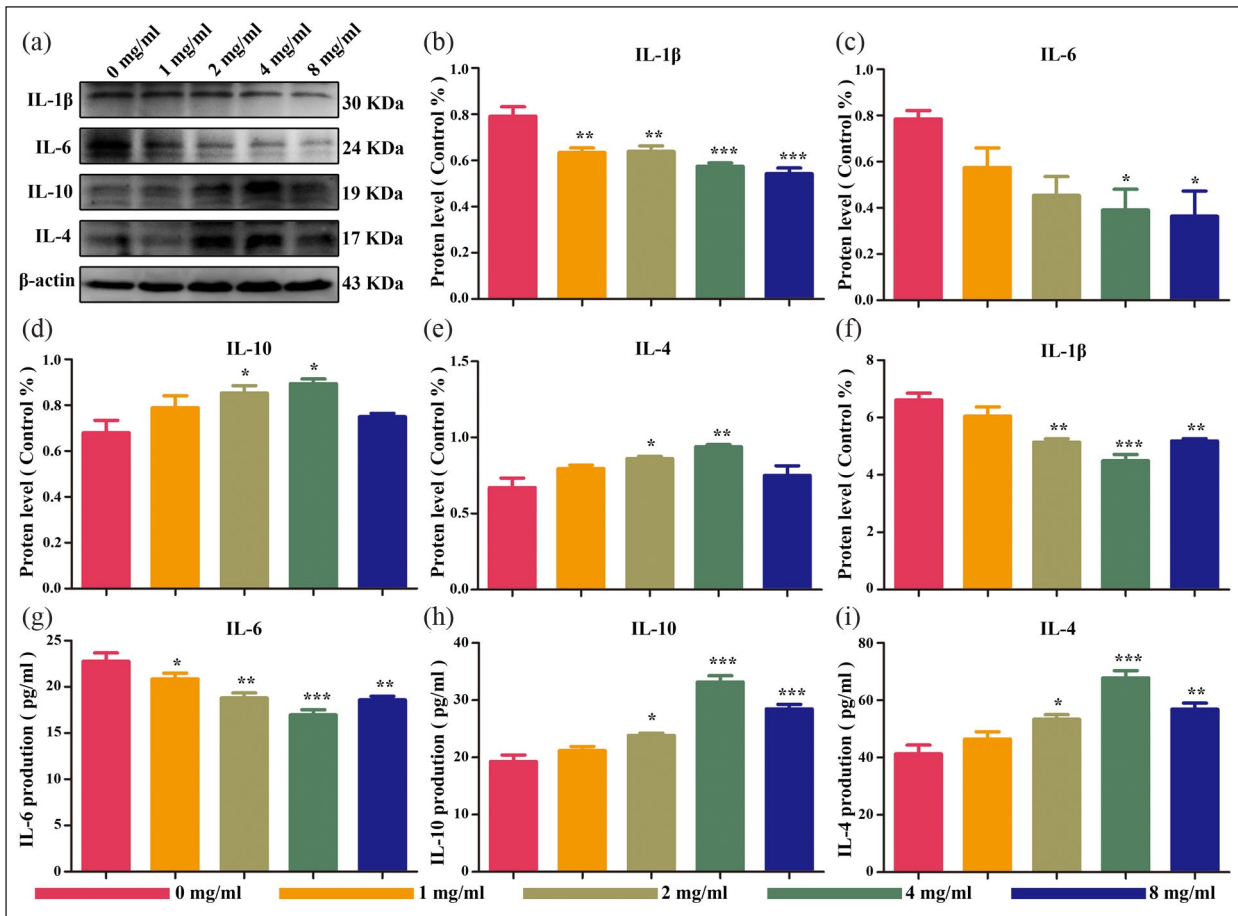


Figure 5. Protein expression of NPCs encapsulated in composite hydrogel scaffolds in the inflammatory microenvironment at 5 days *in vitro*: (a) western blotting of inflammatory factors (IL-1 β , IL-6, IL-10, and IL-4), (b–e) protein expression of inflammatory factors by semi-quantification of western blotting, and (f–i) protein expression of inflammatory factors by semi-quantification of ELISA (compared with the control group, * $p < 0.05$. ** $p < 0.01$. *** $p < .001$).

of the fucoidan-DexMA hydrogel, the inflammatory environment of IDD was modeled by the inflammatory stimulation of NPCs using IL-1 β , in addition to performing a Western blot assay (Figure 5(a)). The results showed that the expression of the pro-inflammatory factors IL-1 β and IL-6 gradually decreased alongside increasing fucoidan concentration (Figure 5(b) and (c)). On the other hand, when the concentration of fucoidan was below 4 mg/ml, the expression of IL-10 and IL-4, which have anti-inflammatory effects, gradually increased with an increase in its concentration, reaching the highest expression at a concentration of 4 mg/ml. However, when the fucoidan concentration was higher than 4 mg/ml, the expression of IL-10 and IL-4 began to decrease (Figure 5(d) and (e)). Another ELISA was then performed on IL-1 β -stimulated NPCs, which found the same experimental results as those of the western blot assay (Figure 5(f)–(i)). Thus, here we hypothesize that the composite hydrogel slowed down the progression of degeneration *in vitro* by inhibiting the expression of anti-inflammatory factors and promoting the expression of anti-inflammatory factors, of which the

scaffold with a fucoidan concentration of 4 mg/ml exhibited the optimal anti-inflammatory effect.

CAV1-YAP signaling pathway involved in the mechanical transduction. The CAV1-YAP signaling pathway modulated cell proliferation and outer matrix protein expression in NPCs by regulating YAP activity, which consequently altered the mechanical strength and structure of the scaffold. Therefore, to evaluate the potential contribution of the CAV1-YAP signaling pathway to the structural mechanotransduction of fucoidan-DexMA hydrogel scaffolds, NPCs were cultured using these composite hydrogel scaffolds containing different concentrations of fucoidan, whilst immunofluorescence staining was performed for YAP and CAV1 (Figure 6(a)). Red fluorescence was used for YAP labeling, DAPI (blue fluorescence) was used to localize the nucleus, and the YAP localized in the extranuclear cytosol was considered to have been in a phosphorylated state, denoted as p-YAP. The percentage of nuclear-localized YAP was then quantified. The fluorescence images illustrated that YAP was mostly in the

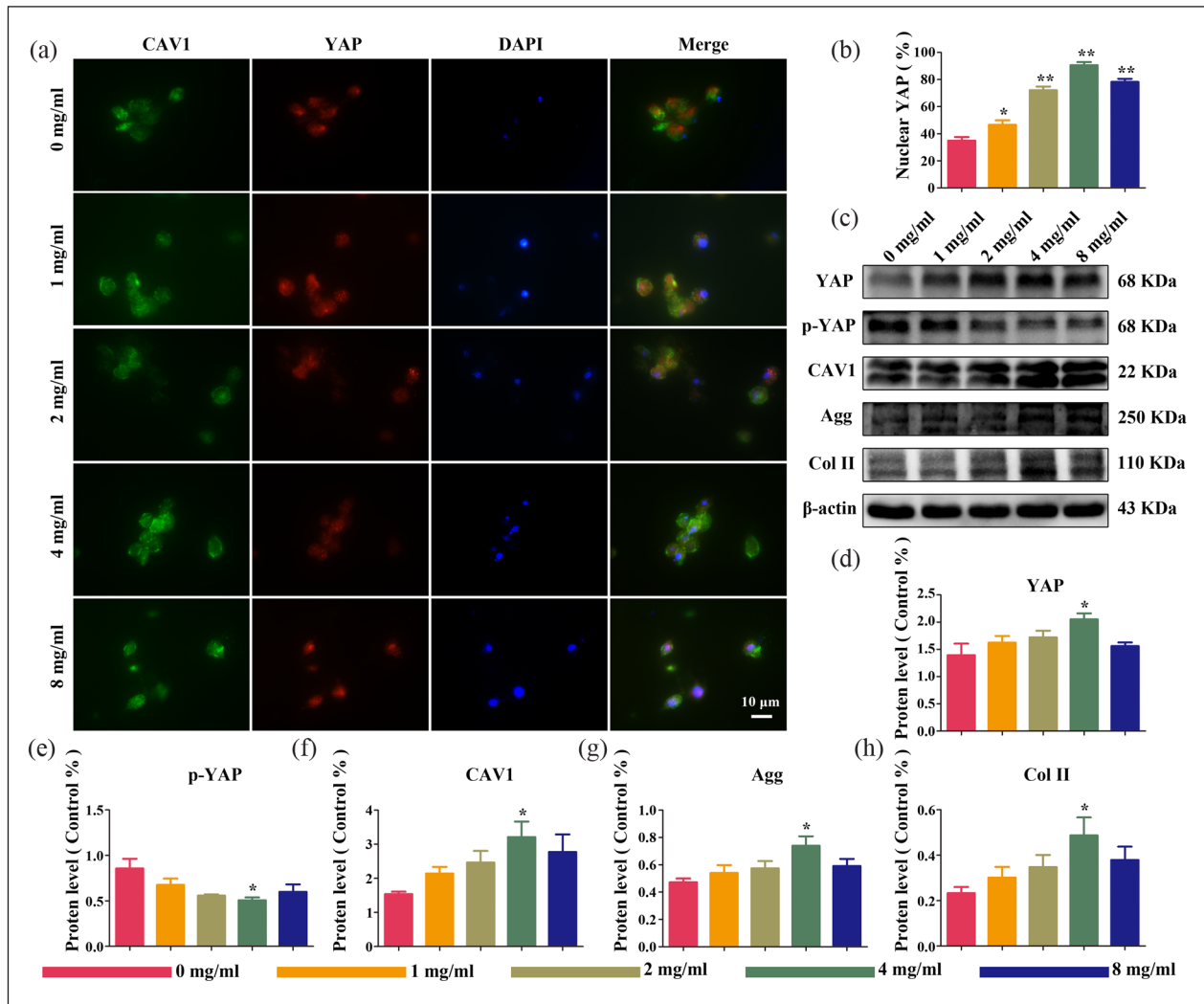


Figure 6. The substrate topography of fucoidan-DexMA composite hydrogel modulates the mechanotransduction process of NPCs through CAV1-YAP regulation: (a) immunofluorescence imaging of CAV1 (green), YAP (red), and DAPI (blue) in cells cultured in fucoidan-DexMA, (b) quantitative analysis of YAP nuclear translocation ratios in cells, (c) expression of CAV1, p-YAP, YAP, Aggrecan, Col II, and β -actin in NPCs cultured in composite hydrogel scaffolds of various concentrations, (d–h) protein expression result of CAV1, P-YAP, YAP, Aggrecan, Col II, and β -actin in NPCs by semi-quantification of western blot cultured in composite hydrogel scaffolds (compared with the control group, * $p < 0.05$. ** $p < 0.01$. *** $p < 0.001$).

phosphorylated state (p-YAP) in the cytosolic membrane when the concentration of fucoidan in the composite hydrogel was at 0 mg/ml. The amount of dephosphorylated YAP localized in the nucleus increased with increasing fucoidan concentration (from 0 to 4 mg/ml). Quantitative optical density analysis of the fluorescence images (Figure 6(c)) indicated that the highest YAP content in the nucleus was reached at fucoidan concentrations of up to 4 mg/ml, with an increase of approximately 56% compared with that in the control, whereas the YAP content in the nucleus began to decrease at higher fucoidan concentrations. The staining of CAV1 remained consistent with YAP staining. Interestingly, this was also consistent with the trend of previous results regarding compression modulus, which seemed to indicate that changes in the stiffness of the composite hydrogel scaffold affected the expression of CAV1

and the nuclear translocation of YAP in NPCs. To further validate the above results, western blot analysis was used to verify the expression of YAP, p-YAP, and CAV1 in each subgroup (Figure 6(b) and (d–f)), which showed that scaffold structural changes did not alter the total YAP protein level; however, there was a correlation between the degree of phosphorylation of YAP and the concentration of fucoidan contained in the scaffold. With an increasing fucoidan concentration in the composite scaffold, p-YAP started to dephosphorylate and translocate to the nucleus, with the highest expression of YAP in the nucleus at a concentration of 4 mg/ml. Meanwhile, the expression of CAV1 was maintained in line with that of YAP but was contrary to the above-mentioned expression of p-YAP.

Next, we investigated the impact of the CAV1-YAP signaling pathway on the expression of proteins in the

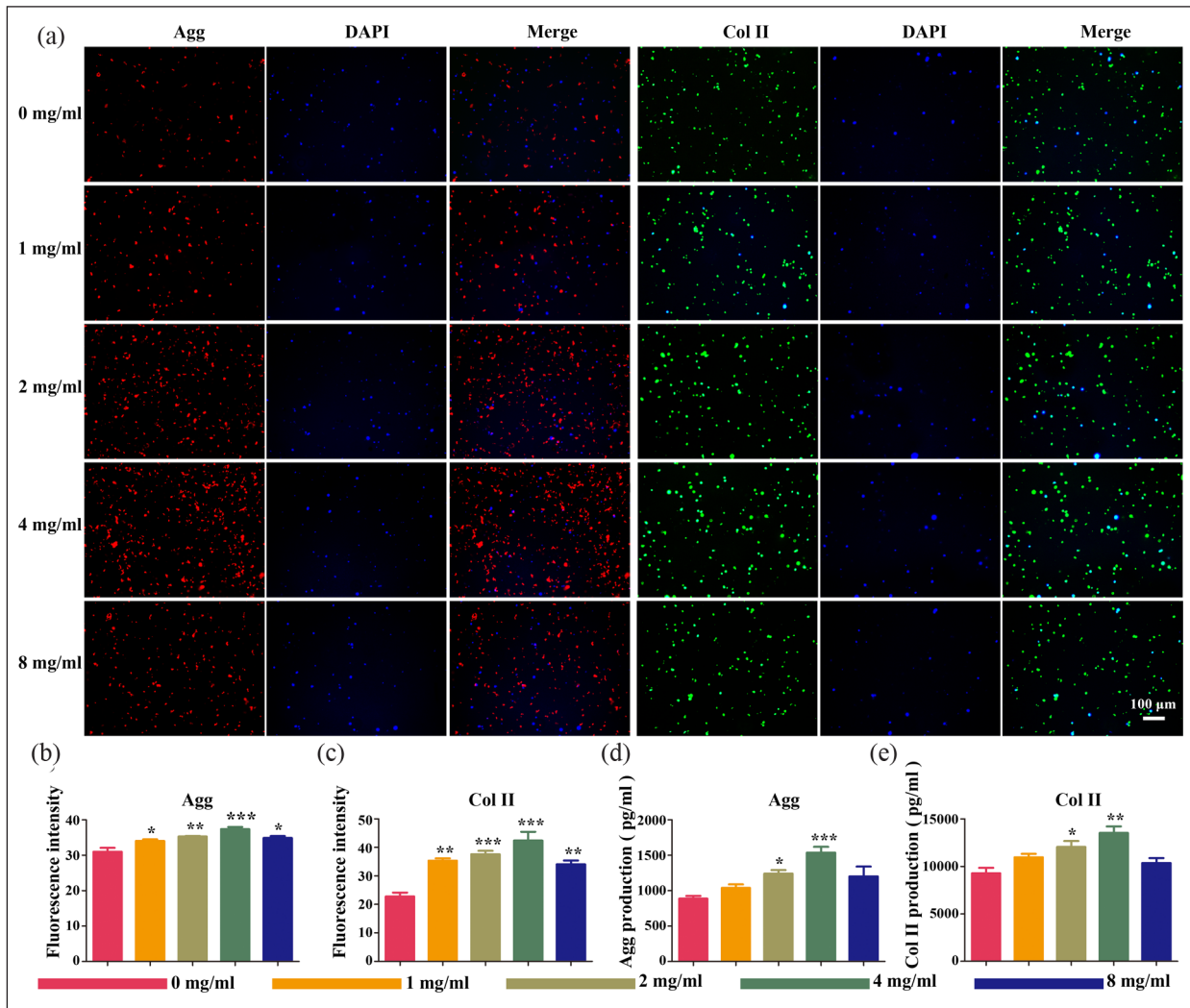


Figure 7. Protein expression of NPCs encapsulated in composite hydrogel scaffolds in the inflammatory microenvironment at 5 days *in vitro*: (a) immunofluorescence imaging of Aggrecan (red), Col II (green), and DAPI (blue) in cells cultured in fucoidan-DexMA. Scale bar 100 μm . (b and c) protein expression of Aggrecan (b) and Col II (c) in NPCs by semi-quantification of immunofluorescence staining. Protein expression of Aggrecan (d) and Col II (e) in NPCs by semi-quantification of ELISA (compared with the control group, * $p < 0.05$. ** $p < 0.01$. *** $p < 0.001$).

outer matrix of NPCs, by incubating NPCs on scaffolds of different levels of stiffness and pore sizes and assaying the protein expression of Col II and Aggrecan, the products of the CAV1-YAP signaling pathway, both of which are also major components of the ECM, where NPCs are embedded. First, we performed immunofluorescence staining (Figure 7(a)) and quantified the optical densities of Aggrecan and Col II (Figure 7(b)). The results of this suggested that the expression of Aggrecan and Col II also increased significantly in parallel with an increase in fucoidan concentration ($p < 0.05$). In subsequent ELISA assays (Figure 7(d) and (e)) and western blot analysis (Figure 6(g) and (h)), the same commonality was confirmed. This indicated that stiffer scaffolds induced CAV1 activation and contributed to YAP translocation to the

nucleus, which in turn regulated the expression of downstream genes, promoting Aggrecan and Col II protein expression, and subsequently the increase in ECM content.

In vivo evaluation

X-ray examination and MRI analysis. Experimental *in vitro* studies previously determined the ability of the fucoidan-DexMA composite hydrogel to regulate cell proliferation and the expression of exosomal proteins in NPCs through its anti-inflammatory mechanism, as well as the CAV1-YAP signaling pathway. To evaluate the *in vivo* potential of fucoidan-DexMA composite hydrogel treatment, an IDD model was constructed, and five groups of hydrogel

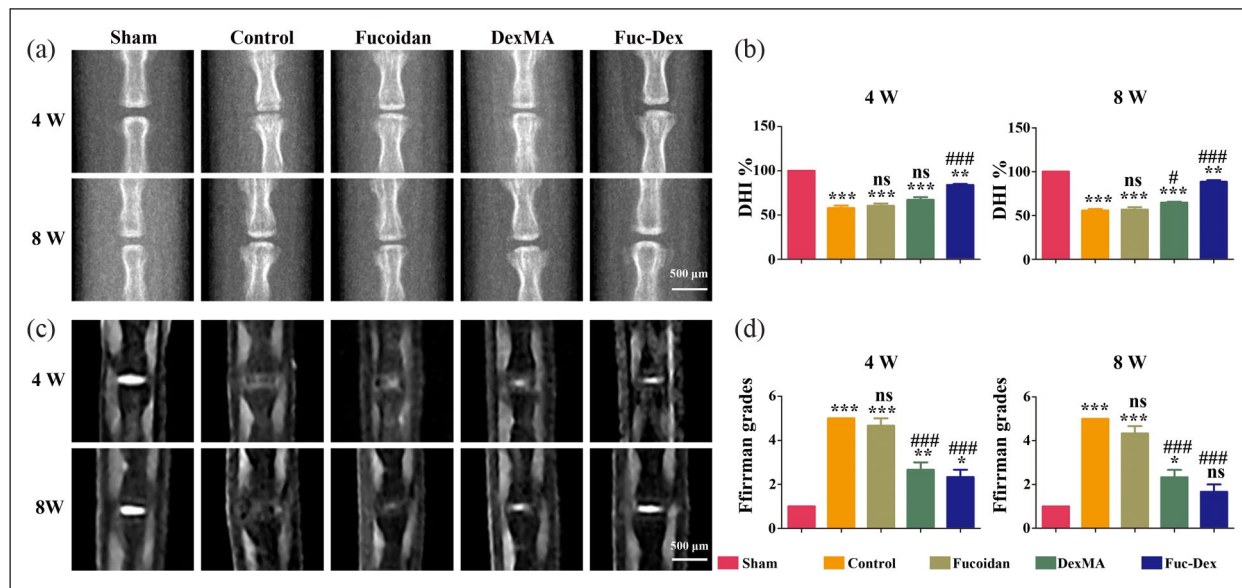


Figure 8. X-ray and MRI evaluation of each group at 4 and 8 weeks post-operation: (a) representative X-ray images of postoperative Co6/Co7 intervertebral discs, (b) DHI %, (c) representative MRI showing the IVD signal intensity, (d) MRI grade statistics. (* $p < 0.05$. ** $p < 0.01$. *** $p < 0.001$ vs sham group, # $p < 0.05$. ### $p < 0.01$. #### $p < 0.001$ vs control group, ns indicates no significant difference).

materials were injected into the NP site to cure the gel: sham, control, fucoidan, DexMA, and Fuc-Dex groups. Throughout the study period, no adverse reactions to implantation were observed in any animal. Imaging was performed after 4 and 8 weeks using radiography and MRI, respectively.

As shown in the radiographs (Figure 8(a)), the IVD height was significantly lower in the control group after the formation of the disc defect than in the sham group. The IVD height was restored to some extent in the fucoidan implantation, DexMA, and Fuc-Dex groups. The results of the assessment using the DHI % (Figure 8(b)) showed that the decrease in disc height observed in the fucoidan and DexMA groups were less than that of the control group. Degenerative disc height recovery was optimal for the Fuc-Dex group, whilst the height at week 8 was significantly greater than that at week 4.

MRI analysis is the gold standard technique used for diagnosing IVD (Figure 8(c)). Healthy discs with a high water content NP were observed to have a high T2-weighted signal in MRI analysis and appear as white healthy disc tissue; however, the destruction of NP led to a significant loss of proteoglycan that disrupted water retention in the IVD, with severe tissue degeneration and “black discs.” At weeks 4 and 8, the control group showed a significantly lower T2-weighted signal in the NP, while the sham group maintained high water. As mentioned previously, the T2-weighted signal can reflect the water content of the NP and thus assess the degree of damage to the NP to some extent, with the results of its quantitative analysis being shown in Supplemental Figure S5. MRI images were further scored

according to Pfirrmann MRI grading (Table S1), the most commonly used for the degree of disc degeneration, yielding a more accurate indication of the recovery of degenerated discs for the different groups (Figure 8(d)). Significantly, the Fuc-Dex group showed the least difference in MRI grading from the sham group at week 8, with no significant difference ($p > 0.05$), demonstrating superior recovery.

Macrophage polarization and secretion of inflammatory cytokines. To assess the aggregation and polarization of macrophages in degenerative IVD tissues, we used sections of rat caudal IVDs at week 4 for immunohistochemical analysis to determine the expression of CCR7, Arg1, and CD68 that label M1, M2, and M0 macrophages, respectively (Figure 9(a)–(c)). Metric analysis revealed that the ratio of CCR7- and CD68-positive cells in the tissue samples of the control group was significantly higher than that of the sham group ($p < 0.01$. $p < 0.001$). However, unlike the control group, the Fuc-Dex group showed a significant decrease in the CCR7- and CD68-positive cell ratio ($p < 0.01$. $p < 0.001$, Figure 9(a), (c), (d), and (f)), while the Arg1-positive cell ratio was significantly higher, Figure 9(b) and (e)). These results indicated that the infiltration and aggregation of M1 and M2 polarized macrophages were observed in the IVDs of the remaining modeling groups, unlike the sham group, whereas fewer M1 polarized macrophages and more M2 polarized macrophage aggregates were present in the IVD tissues of the Fuc-Dex group.

On this basis, we further examined the secretion of inflammatory mediators four weeks after puncture by

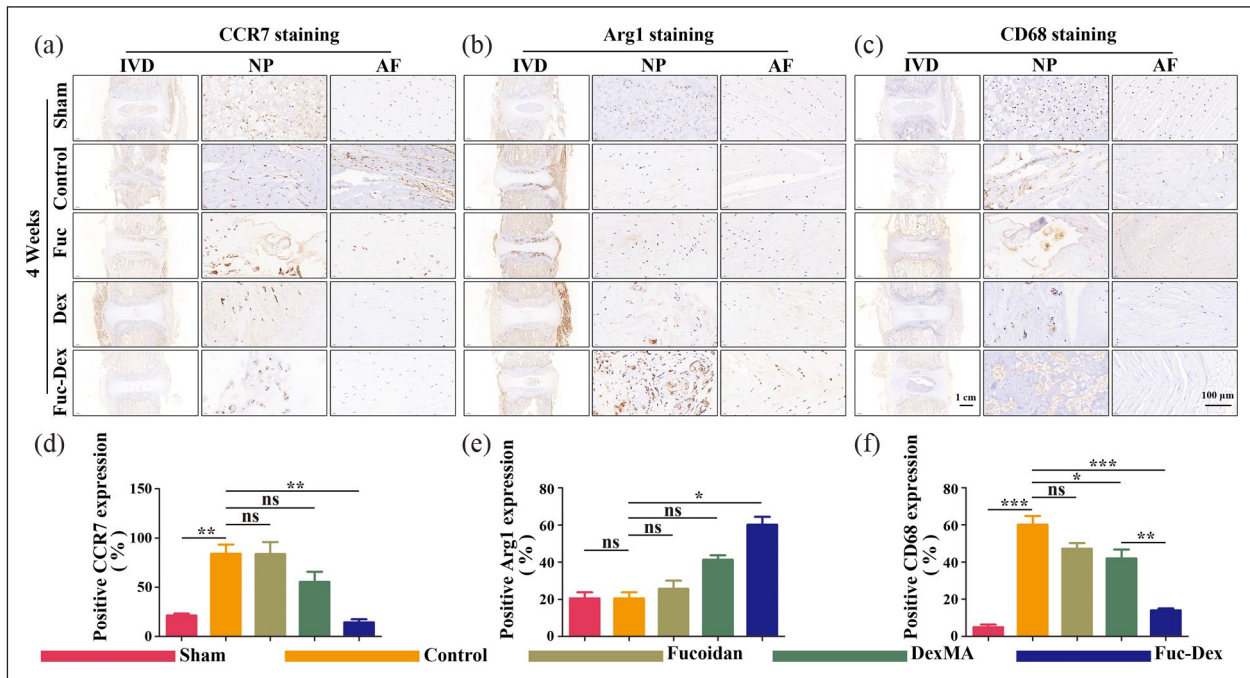


Figure 9. Immunohistochemical (IHC) staining at 4 weeks post-surgery *in vivo*: (a–c) representative images of CCR7, Arg1, and CD68 staining, (d–f) Quantitative analysis of CCR7, Arg1, and CD68-positive cells at 4 weeks after the operation ($*p < 0.05$, $**p < 0.01$, $***p < 0.001$, ns indicates no significant difference).

IHC staining (Figure 10). Compared with the sham group, the percentage of cells positive for the pro-inflammatory mediators IL-1 β and IL-6 was significantly higher in the tissue samples of the control group, whereas the percentage of cells positive for the anti-inflammatory mediators IL-10 and IL-4 showed no significant changes ($p < 0.01$, Figure 10(a) and (b)). In contrast, the ratio of IL-1 β and IL-6 positive cells was significantly reduced for the Fuc-Dex group compared with that of the control group ($p < 0.01$, Figure 10(c) and (d)), whereas the ratio of IL-10 and IL-4 positive cells significantly increased. It can be inferred that the fucoidan-DexMA composite hydrogel scaffold promoted M2 macrophage polarization whilst inhibiting M1-type polarization in IVD tissues with IDD, which in turn enhanced the secretion of anti-inflammatory mediators and inhibited the secretion of pro-inflammatory mediators, thereby creating an anti-inflammatory microenvironment.

Evaluation of IVD regeneration *in vivo* by composite hydrogel. Histological sections were collected at 4 and 8 weeks postoperatively, and the ability of the fucoidan-DexMA composite hydrogel scaffold to promote disc regeneration was further confirmed using IVD histological analysis.

Initially, the IVD morphology was observed using H&E staining (Figure 11(a) and (b)), which showed that from 4 to 8 weeks, the NP of the disc gradually fractured with indistinguishable borders, whilst the NP region was gradually replaced by the fibrous ring in the control and fucoidan

groups. The repair of disc tissue degeneration and structural damage in the DexMA group was better than that observed in the first two groups. Remarkably, the Fuc-Dex group showed a clearer boundary between the NP and the fibrous ring, alongside a significantly higher NP content than that in the other experimental groups. The contrast between the distribution of proteoglycan (blue) and collagen (Sirius red) in the NP of the IVD and the microscopic tissue could be seen more clearly with Safranin O/fast green staining (Figure 11(a) and (b)), which also revealed that NP was gradually being replaced by collagen (Sirius red) in the fucoidan groups. In contrast, the boundary between the Fuc-Dex and Dex groups, especially the Fuc-Dex group, was obvious, which showed the NP regeneration of the IVD. Furthermore, histological scoring of the degenerative changes showed no significant difference between the Fuc-Dex and sham groups after the eighth week of recovery, although the Fuc-Dex group scored significantly higher than the sham group in the fourth week. This further clarified the powerful repair effect of the fucoidan-DexMA composite hydrogel scaffold on degenerated discs.

Finally, the expression of two major components, Aggrecan and COL-II, in NP cells of IVD tissue was further assessed by immunohistochemical staining of histological sections at 4 and 8 weeks postoperatively, with the results consistent with the histological analysis (Figure 12). The levels of Col II and Aggrecan in the Fuc-Dex group were significantly higher at 4 weeks than those in

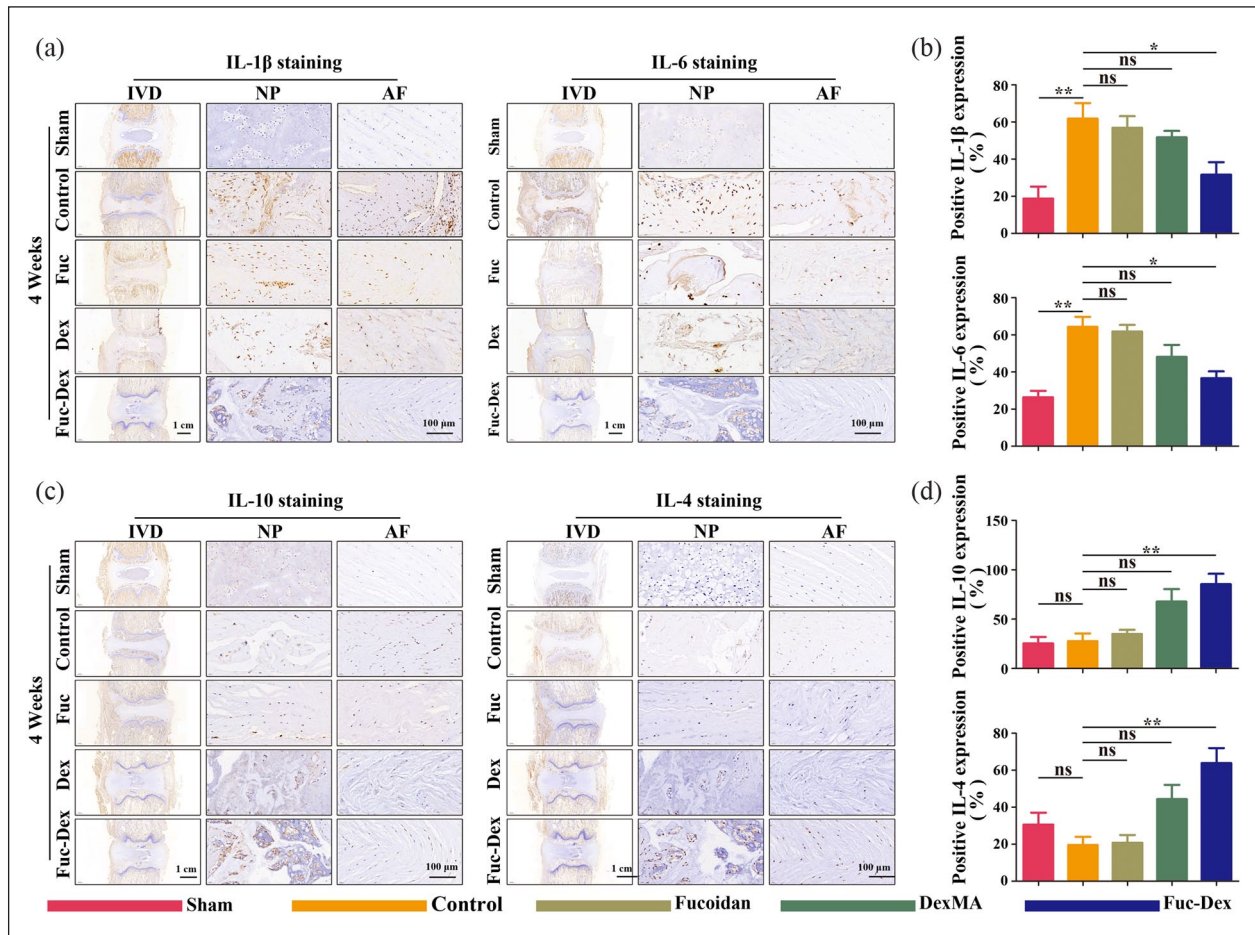


Figure 10. IHC staining at 4 weeks after the operation *in vivo*: (a) representative images of IL-1 β and IL-6 staining. (b) quantitative analysis of IL-1 β and IL-6 staining positive cells. (c) representative images of IL-10 and IL-4 staining. (d) quantitative analysis of IL-10 and IL-4 staining positive cells. (* $p < 0.05$. ** $p < 0.01$. *** $p < 0.001$, ns indicates no significant difference).

the control, fucoidan, and Dex groups, but lower than those in the sham group (Figure 12(a) and (b)). At 8 weeks, Col II and Aggrecan levels in the Fuc-Dex group were no longer significantly different from those in the sham group (Figure 12(c) and (d)). These results show the promoting effect of the fucoidan-DexMA composite hydrogel scaffold on the tissue regeneration of degenerative discs.

Discussion

The IVD is important in the movement and essential stability of the spine and thus is irreplaceable. Currently, the available mainstream invasive surgical treatments have limited effectiveness alongside a risk of injury; therefore, an alternative, simple, and effective treatment is urgently needed. Tissue engineering of NP provides a viable avenue for the treatment of IVD degeneration, owing to the avascular nature of NP tissues and the unsuitability of oral administration for IDD treatment.^{18,37} In recent years, encouraging achievements have been reported in terms of the promotion of disc tissue regeneration with the

assistance of tissue-engineering approaches.^{38–40} Given that the inflammatory microenvironment plays a crucial role in the development and progression of IDD, the local injection of anti-inflammatory hydrogels appears to present a promising therapeutic strategy.^{41–43} This study constructed a fucoidan-DexMA polysaccharide composite hydrogel that could be injected into the NP and thus effectively repaired the IVD structure based on the mechanical and anti-inflammatory properties of the material.

From the results of the material characterization tests, ¹H NMR spectra confirmed the successful synthesis of DexMA. We then mixed fucoidan into DexMA hydrogels to synthesize fucoidan-DexMA polysaccharide composite hydrogels. Fucoidan contains a sulfate group, which is mainly substituted on C-2 and C-4, and occasionally on C-3, giving fucoidan a negative charge.⁴⁴ To some extent, this mimics the natural NP organization which contains negatively charged sulfated glycosaminoglycans (sGAGs).⁴⁵ The SEM photograph shows the classical porous honeycomb structure of the fucoidan-DexMA polysaccharide composite hydrogel, where the encapsulated

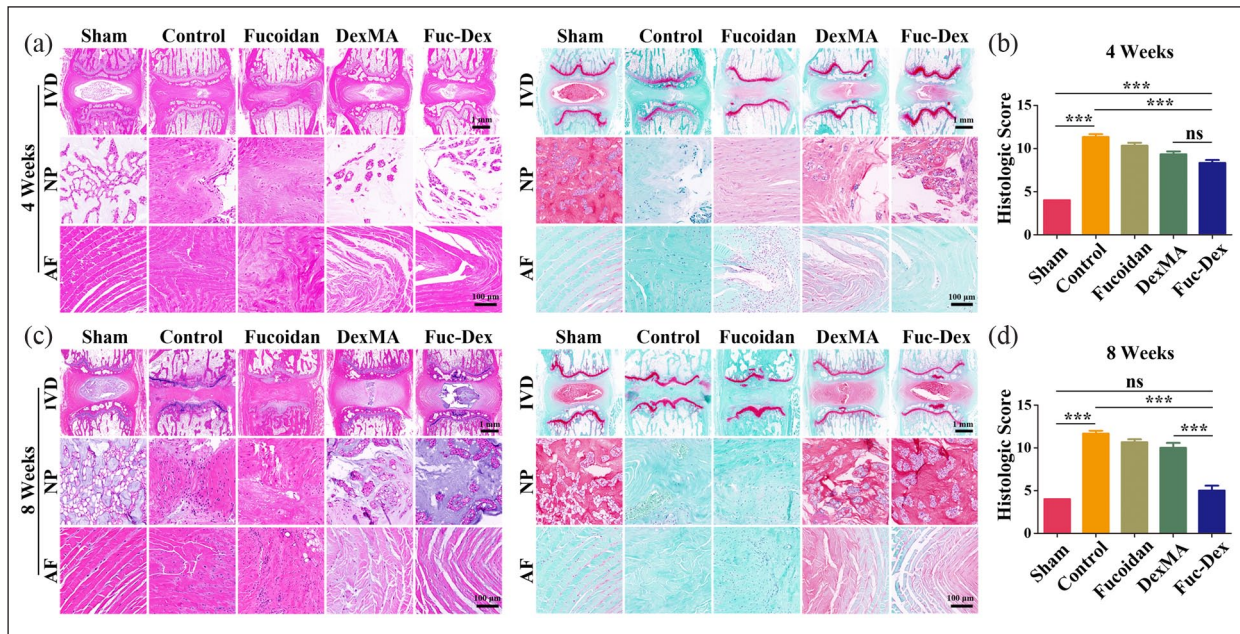


Figure 11. Histological staining at 4 and 8 weeks after a puncture *in vivo*: (a) representative paraffin section with H&E and Safranin O/fast green staining at 4 weeks, (b) Histological grading was determined at 4 weeks, (c) representative paraffin section with H&E and Safranin O/fast green staining at 8 weeks, (d) Histological grading was determined at 8 weeks. (In H&E staining, the collagen deposits are shown as a darker pink color, while in Safranin O/fast green staining, the collagen deposits are shown as a Sirius red color; * $p < 0.05$. ** $p < 0.01$. *** $p < 0.001$, ns indicates no significant difference).

of fucoidan into the DexMA gels can be observed to exhibit smaller and tighter honeycomb structures. This can probably be ascribed to the hydrogen bonding structure formed between the hydroxyl group of fucoidan and dextran.^{46,47} Meanwhile, the WCA assay confirmed the hydrophilic properties of the fucoidan-DexMA polysaccharide composite hydrogels. The classical porous structure and strong hydrophilicity of this hydrogel have been proven to facilitate nutrient exchange, thus contributing to a highly favorable microenvironment for the encapsulated cells. Moreover, this provides space for cell proliferation and cytosolic extension, thus facilitating the growth of NP cells and the regeneration of IVD tissues.

A high density of negatively charged proteoglycan (PG) molecules offers the ability to absorb approximately triple their weight in water, thereby allowing NP to be mechanically resilient under compressive loading.⁴⁸ The fucoidan-DexMA polysaccharide composite hydrogel scaffold, which is also negatively charged, should theoretically possess similar mechanical properties. As predicted, in the compression modulus test performed on the composite hydrogel scaffold, the composite hydrogel scaffold mixed with 4 mg/ml had a compression modulus of 10.42 ± 2.07 kPa, which also reached the mechanical strength required for natural discs (5–35 kPa),^{49–51} thus demonstrating favorable mechanical properties. The compression modulus of the composites showed a decrease when the fucoidan was incorporated at a concentration of 8 mg/ml, which may be due to the excess of fucoidan,

resulting in the repulsion of the negatively charged sulfate groups contained therein, hence playing a negative role in the binding of the composite material and thus its properties.

Interestingly, when cell viability assays were performed on fucoidan-DexMA polysaccharide composite hydrogel scaffolds mixed with different concentrations of fucoidan, we found that the 4 mg/ml group of scaffolds with the highest compression modulus displayed the greatest dominance in terms of cell proliferation capacity and cell viability. Thus, we concluded that the stiffness and structure of the matrix may have affected the proliferation and activity of NPCs. Previous studies have indicated that cells can sense the mechanical strength of the ECM through the Hippo pathway effector YAP and its transcriptional coactivator PDZ-binding motif (TAZ), which profoundly influences cell behavior. YAP is present in the cytoplasm in an inactivated phosphorylated form under mechanical conditions that produce low contractile forces in the cells.^{52,53} Conversely, it is dephosphorylated and relocalized to the nucleus, where it can regulate gene expression and thus remodel the ECM. Furthermore, CAV1, an integral membrane protein that coordinates multiple signals on the cell surface, has been reported to control actin contraction and organization through Rho and responds to different types of mechanical stimuli such as shear stress, stretching, and substrate stiffness, whilst participating in mechanical transduction processes. It has been previously reported that annulus fibrosus-derived stem cells induced by

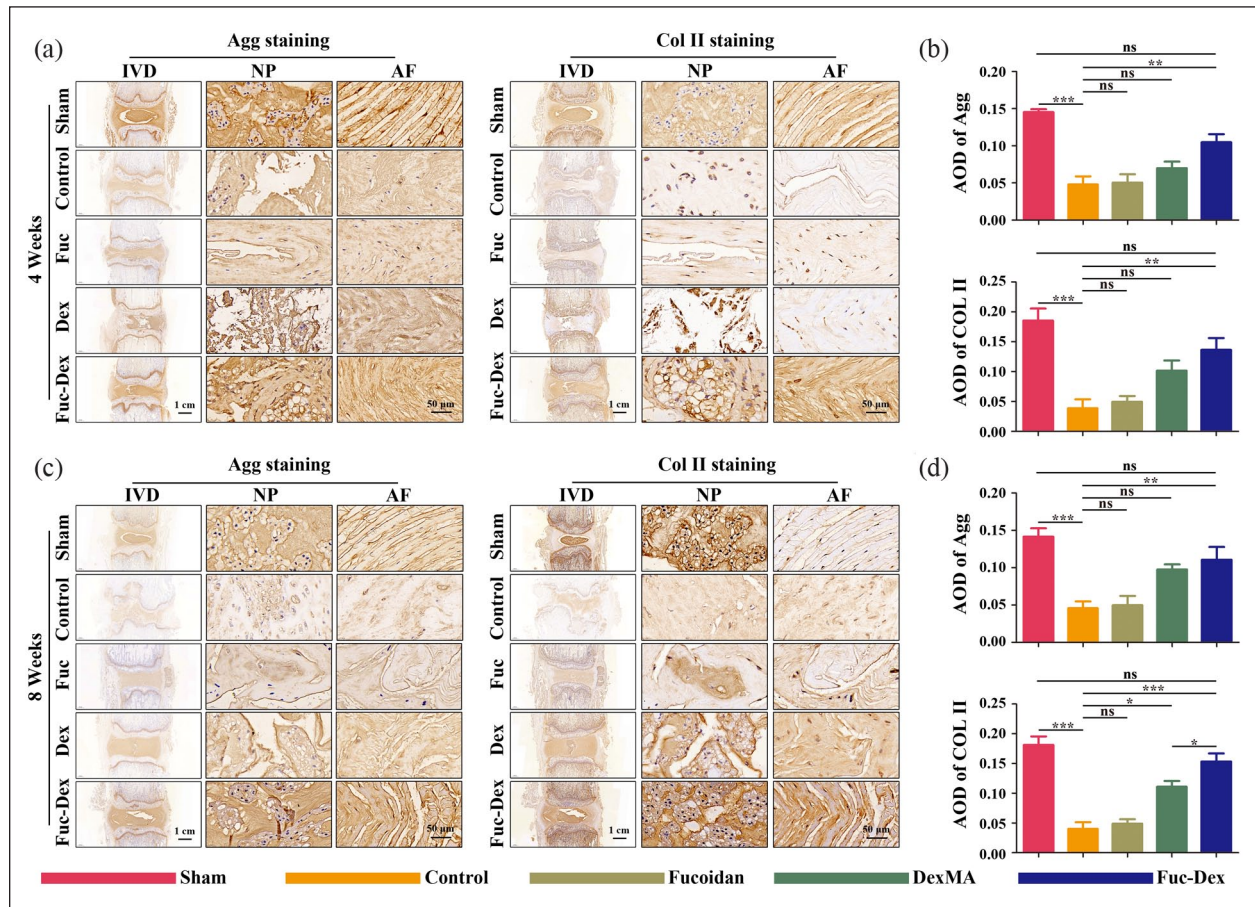


Figure 12. IHC staining of Agg and Col II at 4 and 8 weeks after the operation *in vivo*: representative images of Agg and Col II staining at 4 (a) and 8 weeks (c) postoperatively. (b) Analysis of average optical density (AOD) values at 4 (b) and 8 weeks (d) postoperatively. (* $p < 0.05$, ** $p < 0.01$, *** $p < 0.001$, ns indicates no significant difference).

stiffness and structure, among others, modulated YAP activity through CAV1 by controlling the nucleoplasmic shuttle of YAP, which in turn regulated the cellular activity and ECM expression.³⁰

Therefore, we propose that altering the mechanical strength and structure of scaffolds may regulate cell proliferation and outer matrix protein expression in NPCs through the CAV1-YAP signaling pathway. We also assayed the protein expression of CAV1, YAP, p-YAP, Col II, and Aggrecan in cells cultured on scaffolds with different levels of stiffness and pore sizes. The results verified our assumption that the YAP content localized in the nucleus increased by approximately 56% when the compression modulus was changed from 7.31 ± 1.88 kPa (control group) to 10.42 ± 2.07 kPa (4 mg/ml group; Figure 6(a)). Additionally, the corresponding YAP protein expression was shown to have significantly increased by western blot assay, whilst the expressions of CAV1, Aggrecan, and Col II were all significantly increased. Aggrecan and Col II levels were also significantly increased simultaneously ($p < 0.05$; Figure 6(d)–(h)). This indicated that the stiffer scaffold induced CAV1 activation and YAP translocation

to the nucleus, which in turn regulated the expression of downstream genes and promoted the protein expression of Aggrecan and Col II. The expression of p-YAP gradually decreased with increasing scaffold stiffness during this process, further confirming the validity of this conclusion.

One previous study suggested that fucoidan decreased the mRNA expression levels of inflammation-related genes and increased the expression of ECM genes such as *Col IIa1* and *Acan* in IVD-derived fibroblasts in an inflammatory environment.¹⁸ However, it is unclear whether fucoidan had the same effect on NPCs in IVD. IL-1 β is one of the most critical pro-inflammatory factors associated with the initiation and progression of DDD that triggers higher levels of pro-inflammatory mediators (including TNF- α , IL-6, and some matrix-degrading enzymes),^{33,54,55} which disrupt ECM metabolic homeostasis and impair metabolism.^{56,57} We simulated the tissue environment of degenerating IVD using an *in vitro* environment containing IL-1 β and performed a cell live/death assay, which demonstrated that the cell proliferation and activity of NPCs positively correlated with the concentration of fucoidan in the scaffold below

4 mg/ml. This implied that an appropriate concentration of this composite hydrogel could promote the proliferation and ECM recovery of NPCs in the inflammatory environment after IL-1 β treatment through an anti-inflammatory effect. Consequently, the subsequent western blotting results showed that after IL-1 β treatment, NPCs encapsulated in the fucoidan-DexMA polysaccharide complex hydrogel showed not only decreased expression of IL-1 β and IL-6 pro-inflammatory factors but also elevated protein levels of anti-inflammatory factors IL-10 and IL-4. These results indicated that appropriate concentrations of fucoidan-DexMA hydrogel scaffolds could inhibit inflammatory effects and regulate cell behavior, which in turn, would promote proliferation and ECM protein expression in NPCs.

In subsequent animal experiments and histological analyses, the mechanisms by which fucoidan-DexMA polysaccharide complex hydrogels counteracted inflammation were investigated in detail. During DDD, macrophage infiltration, differentiation, and secretion of cytokines complement or synergize with the regulatory effects of NPCs.⁵⁸ Resting-state macrophages (M0) undergo two different polarizations in this environment: M1 and M2. Specifically, M1 inhibits NPC proliferation and exacerbates IDD degeneration, whereas M2 attenuates DDD development.^{6,59,60} M1 exacerbates IDD by inhibiting cell proliferation and cellular anabolism and contributes to the secretion of pro-inflammatory mediators, in contrast to M2, which exhibits protective effects by inhibiting inflammatory factor-induced ECM degradation and inflammatory responses. Immunohistochemical staining showed that CCR7 (a marker of M1) expression was significantly increased at 4 weeks post-operation, whereas Arg1 (a marker of M2) expression significantly decreased at this time. This confirmed the ability of fucoidan-DexMA polysaccharide complex hydrogels to regulate the inflammatory microenvironment associated with macrophage polarization. Moreover, as reflected by the immunohistochemical staining analysis of Aggrecan and Col II in ECM, Fuc-Dex groups showed significantly higher levels of expression than did all other groups. The collagen content recovered by week 8 and was not significantly different from that observed in the sham group. It was concluded that the fucoidan-DexMA polysaccharide complex hydrogel effectively regulated the inflammatory microenvironment of the IVD during degeneration to maintain the metabolic balance of the ECM within the NP, which in turn promoted the regeneration of IVD tissues.

The imaging analysis showed that gradual recovery of the degenerated disc height in the Fuc-Dex group was observed, whilst the T2-weighted signal in the MRI of the Fuc-Dex group was able to maintain a higher level. In addition to the subsequent histological staining, it was found that the composite hydrogel scaffold could not only maintain and restore the high water content of the NP cells

but also effectively promote the regeneration of the degenerated disc, with the histological score progressively approaching that of the sham group. All these results provided considerable visual proof that the fucoidan-DexMA composite hydrogel scaffold was able to reverse disc tissue degeneration and structural damage, thus promoting degenerative disc regeneration.⁶¹

The MRI images demonstrated a high T2-weighted signal similar to that of the sham-operated group, indicating a healthy disc with a high water-content nucleus pulposus. Moreover, by H&E staining and Safranin O-fast green staining, collagen tissue ingrowth was observed, implying the reconstruction of the nucleus pulposus tissue with favorable compression properties. The primary function of the IVD is to conduct the mechanical stress to the spine, holding the active junction for spinal flexion, stretching, and other activities.⁶² And the compression properties are largely related to the function of IVD, such as bending and compression function.⁴⁸ Having favorable compression properties indicates a good functional recovery of the IVD.

In-depth cellular and animal studies in this experiment demonstrated the superior performance of the fucoidan-DexMA composite hydrogel scaffold. In addition, this tissue engineering material, which can be injected directly into the NP, avoids the necessity for complex and risky surgical procedures. Compared with previous hydrogel research strategies, in which the importance of the anti-inflammatory microenvironment to promote integrated disc repair in natural tissues was frequently overlooked, this unique hydrogel strategy not only combines the immunomodulatory properties of fucoidan gels, but also leverages the advantages of tissue-engineered scaffold bionic structures to restore the structure of the NP and disc height in spinal segments. The incorporation of the negatively charged fucoidan component gives the hydrogel scaffold similar rheological properties to NP, and experiments have also demonstrated its excellent biocompatibility and safety. So it may provide new insight into the clinical repair of disc degeneration. Nevertheless, the limitations and drawbacks of this study still exist. We used the rat IDD model in which the pathological progression is more rapid than that in humans, and the pathogenesis of DDD is a complex process involving many relevant factors; therefore, the simulation of clinical disc degeneration recovery is not perfectly accurate. Therefore, the *in vivo* therapeutic efficacy of this scaffold for DDD in the inflammatory setting remains to be further explored.

Conclusion

In this study, as a result of adding fucoidan with a negative charge and anti-inflammatory effects to DexMA, we successfully assembled a fucoidan-DexMA composite hydrogel scaffold to regulate ECM metabolic homeostasis, inhibit inflammation, and restore tissue function. *In vivo*

and *ex vivo* experiments showed that the scaffold increased the proliferation of NPCs whilst enhancing the synthesis of ECM on NPCs via the CAV1-YAP signaling pathway. Specifically, it upregulated the expression of Aggrecan and Col II and enhanced ECM deposition in the long term. In addition, it promoted the M2 polarization of infiltrating macrophages and effectively alleviated the inflammatory microenvironment. These processes significantly inhibited IDD and promoted tissue regeneration. Moreover, the recovery effect on the degenerated discs was fully validated in animal experiments. Therefore, it can be concluded that this injectable polysaccharide-composite hydrogel scaffold presents a new strategy for the regeneration of IDD tissues in a hyperinflammatory local microenvironment. These results provide new ideas for the tissue engineering approach to IDD repair, but the prospects of their clinical application still should be further explored.

Author contributions

LWF: Conceptualization, Methodology, Data curation, Writing-original draft. ZPH: Methodology, Investigation, Data curation, Funding acquisition, Writing-original draft. YBM: Methodology, Investigation, Data curation, Writing-original draft. QMY: Methodology, Investigation, Data curation. CYD: Methodology, Investigation, Data curation. SLJ: Methodology, Investigation. Jianzhong Guan: Conceptualization, Supervision, Validation. ZL: Conceptualization, Supervision, Validation, Project administration, Writing-review & editing. MYJ: Conceptualization, Supervision, Resources, Funding acquisition, Writing-review & editing.

Availability of data and materials

The datasets used and/or analyzed during the current study are available from the corresponding author on reasonable request.

Declaration of conflicting interests

The author(s) declared no potential conflicts of interest with respect to the research, authorship, and/or publication of this article.

Funding

The author(s) disclosed receipt of the following financial support for the research, authorship, and/or publication of this article: This study was supported by grants from the 512 Talents Development Project of Bengbu Medical College (by51202302 and by51202309), the Opening Project of Anhui Province Key Laboratory of Tissue Transplantation in Bengbu Medical College (AHTT2022A001), the Domestic Visiting and Training Program for Outstanding Young Backbone Teachers in High Schools (gxgnfx2022036), the Natural Science Research Project of the Anhui Educational Committee (KJ2021ZD0089 and 2022AH020086), and the Scientific Research Foundation of Bengbu Medical College (2021bypd006).

ORCID iDs

Pinghui Zhou  <https://orcid.org/0000-0002-1141-5987>
Yingji Mao  <https://orcid.org/0000-0001-9737-1526>

Supplemental material

Supplemental material for this article is available online.

Reference

1. Kamatani T, Hagizawa H, Yarimitsu S, et al. Human iPS cell-derived cartilaginous tissue spatially and functionally replaces nucleus pulposus. *Biomaterials* 2022; 284: 121491.
2. Peng Y, Qing X, Lin H, et al. Decellularized disc hydrogels for hBMSCs tissue-specific differentiation and tissue regeneration. *Bioact Mater* 2021; 6: 3541–3556.
3. Zhang Y, Xu Y, Kong H, et al. Microneedle system for tissue engineering and regenerative medicine. *Exploration* 2023; 3: 20210170.
4. Liu G, Bao Z and Wu J. Injectable baicalin/F127 hydrogel with antioxidant activity for enhanced wound healing. *Chin Chem Lett* 2020; 31: 1817–1821.
5. Tan X, Jain E, Barcellona MN, et al. Integrin and syndecan binding peptide-conjugated alginate hydrogel for modulation of nucleus pulposus cell phenotype. *Biomaterials* 2021; 277: 121113.
6. Zhang W, Wang H, Yuan Z, et al. Moderate mechanical stimulation rescues degenerative annulus fibrosus by suppressing caveolin-1 mediated pro-inflammatory signaling pathway. *Int J Biol Sci* 2021; 17: 1395–1412.
7. Newell N, Little JP, Christou A, et al. Biomechanics of the human intervertebral disc: a review of testing techniques and results. *J Mech Behav Biomed Mater* 2017; 69: 420–434.
8. Ni L, Zheng Y, Gong T, et al. Proinflammatory macrophages promote degenerative phenotypes in rat nucleus pulposus cells partly through ERK and JNK signaling. *J Cell Physiol* 2019; 234: 5362–5371.
9. Bian J, Cai F, Chen H, et al. Modulation of local overactive inflammation via injectable hydrogel microspheres. *Nano Lett* 2021; 21: 2690–2698.
10. Sanjeeva KKA, Kim EA, Son KT, et al. Bioactive properties and potentials cosmeceutical applications of phlorotannins isolated from brown seaweeds: a review. *J Photochem Photobiol B* 2016; 162: 100–105.
11. Lu HT, Chang WT, Tsai ML, et al. Development of Injectable Fucoidan and Biological Macromolecules Hybrid Hydrogels for Intra-Articular Delivery of Platelet-Rich Plasma. *Mar Drugs* 2019; 17(4): 236
12. Li T, Yang J, Weng C, et al. Intra-articular injection of anti-inflammatory peptide-loaded glycol chitosan/fucoidan nanogels to inhibit inflammation and attenuate osteoarthritis progression. *Int J Biol Macromol* 2021; 170: 469–478.
13. Borrelli C and Buckley CT. Injectable disc-derived ECM hydrogel functionalised with chondroitin sulfate for intervertebral disc regeneration. *Acta Biomater* 2020; 117: 142–155.
14. Shan H, Gao X, Zhang M, et al. Injectable ROS-scavenging hydrogel with MSCs promoted the regeneration of damaged skeletal muscle. *J Tissue Eng* 2021; 12: 20417314211031378.
15. Kim DS, Kim JH, Baek SW, et al. Controlled vitamin D delivery with injectable hyaluronic acid-based hydrogel for restoration of tendinopathy. *J Tissue Eng* 2022; 13: 20417314221122089.
16. Sumayya AS and Muraleedhara Kurup G. In vitro anti-inflammatory potential of marine macromolecules cross-

- linked bio-composite scaffold on LPS stimulated RAW 264.7 macrophage cells for cartilage tissue engineering applications. *J Biomater Sci Polym Ed* 2021; 32: 1040–1056.
17. Pineiro-Ramil M, Florez-Fernandez N, Ramil-Gomez O, et al. Antifibrotic effect of brown algae-derived fucoidans on osteoarthritic fibroblast-like synoviocytes. *Carbohydr Polym* 2022; 282: 119134.
 18. Yu Q, Han F, Yuan Z, et al. Fucoidan-loaded nanofibrous scaffolds promote annulus fibrosus repair by ameliorating the inflammatory and oxidative microenvironments in degenerative intervertebral discs. *Acta Biomater* 2022; 148: 73–89.
 19. Buckley CT, Hoyland JA, Fujii K, et al. Critical aspects and challenges for intervertebral disc repair and regeneration—Harnessing advances in tissue engineering. *JOR Spine* 2018; 1: e1029.
 20. Ligorio C, O'Brien M, Hodson NW, et al. TGF-beta3-loaded graphene oxide – self-assembling peptide hybrid hydrogels as functional 3D scaffolds for the regeneration of the nucleus pulposus. *Acta Biomater* 2021; 127: 116–130.
 21. Cheng YH, Yang SH and Lin FH. Thermosensitive chitosan-gelatin-glycerol phosphate hydrogel as a controlled release system of ferulic acid for nucleus pulposus regeneration. *Biomaterials* 2011; 32: 6953–6961.
 22. Cai L, Li J, Quan S, et al. Dextran-based hydrogel with enhanced mechanical performance via covalent and non-covalent cross-linking units carrying adipose-derived stem cells toward vascularized bone tissue engineering. *J Biomed Mater Res A* 2019; 107: 1120–1131.
 23. Ding Y, Li Z, Hu W, et al. Carbazate-modified cross-linked dextran microparticles suppress the progression of osteoarthritis by ROS scavenging. *Biomater Sci* 2021; 9: 6236–6250.
 24. Davidson CD, Wang WY, Zaimi I, et al. Cell force-mediated matrix reorganization underlies multicellular network assembly. *Sci Rep* 2019; 9: 12.
 25. Liu J, Long H, Zeuschner D, et al. Synthetic extracellular matrices with tailored adhesiveness and degradability support lumen formation during angiogenic sprouting. *Nat Commun* 2021; 12: 3402.
 26. Pan Y, Xiao Y, Hao Y, et al. An injectable mPEG-PDLLA microsphere/PDLLA-PEG-PDLLA hydrogel composite for soft tissue augmentation. *Chin Chem Lett* 2022; 33: 2486–2490.
 27. Trappmann B, Baker BM, Polacheck WJ, et al. Matrix degradability controls multicellularity of 3D cell migration. *Nat Commun* 2017; 8: 371.
 28. Baker BM, Trappmann B, Wang WY, et al. Cell-mediated fibre recruitment drives extracellular matrix mechanosensing in engineered fibrillar microenvironments. *Nat Mater* 2015; 14: 1262–1268.
 29. Xu P, Guan J, Chen Y, et al. Stiffness of photocrosslinkable gelatin hydrogel influences nucleus pulposus cell properties in vitro. *J Cell Mol Med* 2021; 25: 880–891.
 30. Srivastava A, Isa IL, Rooney P, et al. Bioengineered three-dimensional diseased intervertebral disc model revealed inflammatory crosstalk. *Biomaterials* 2017; 123: 127–141.
 31. Totaro A, Panciera T and Piccolo S. YAP/TAZ upstream signals and downstream responses. *Nat Cell Biol* 2018; 20: 888–899.
 32. Chu G, Yuan Z, Zhu C, et al. Substrate stiffness- and topography-dependent differentiation of annulus fibrosus-derived stem cells is regulated by Yes-associated protein. *Acta Biomater* 2019; 92: 254–264.
 33. Luo X, Huan L, Lin F, et al. Ulinastatin ameliorates IL-1beta-induced cell dysfunction in human nucleus pulposus cells via Nrf2/NF-kappaB pathway. *Oxid Med Cell Longev* 2021; 2021: 5558687.
 34. Wang Y, Wang X, Shang J, et al. Repairing the ruptured annular fibrosus by using type I collagen combined with citric acid, EDC and NHS: an in vivo study. *Eur Spine J* 2017; 26: 884–893.
 35. Hirata H, Yurube T, Kakutani K, et al. A rat tail temporary static compression model reproduces different stages of intervertebral disc degeneration with decreased notochordal cell phenotype. *J Orthop Res* 2014; 32: 455–463.
 36. Keorochana G, Johnson JS, Taghavi CE, et al. The effect of needle size inducing degeneration in the rat caudal disc: evaluation using radiograph, magnetic resonance imaging, histology, and immunohistochemistry. *Spine J* 2010; 10: 1014–1023.
 37. Zhang GZ, Deng YJ, Xie QQ, et al. Sirtuins and intervertebral disc degeneration: roles in inflammation, oxidative stress, and mitochondrial function. *Clin Chim Acta* 2020; 508: 33–42.
 38. Lyu FJ, Cui H, Pan H, et al. Painful intervertebral disc degeneration and inflammation: from laboratory evidence to clinical interventions. *Bone Res* 2021; 9: 7.
 39. Monchaux M, Forterre S, Spreng D, et al. Inflammatory processes associated with canine intervertebral disc herniation. *Front Immunol* 2017; 8: 1681.
 40. Cheng Z, Xiang Q, Wang J, et al. The potential role of melatonin in retarding intervertebral disc ageing and degeneration: a systematic review. *Ageing Res Rev* 2021; 70: 101394.
 41. Sharma S, Sudhakara P, Singh J, et al. Critical review of biodegradable and bioactive polymer composites for bone tissue engineering and drug delivery applications. *Polymers* 2021; 13(16): 2623.
 42. Liu Y, Du J, Peng P, et al. Regulation of the inflammatory cycle by a controllable release hydrogel for eliminating postoperative inflammation after discectomy. *Bioact Mater* 2021; 6: 146–157.
 43. Cui S and Zhang L. microRNA-129-5p shuttled by mesenchymal stem cell-derived extracellular vesicles alleviates intervertebral disc degeneration via blockade of LRG1-mediated p38 MAPK activation. *J Tissue Eng* 2021; 12: 204173142111021679.
 44. Citkowska A, Szekalska M and Winnicka K. Possibilities of fucoidan utilization in the development of pharmaceutical dosage forms. *Mar Drugs* 2019; 17: 458.
 45. Niosi CA and Oxland TR. Degenerative mechanics of the lumbar spine. *Spine J* 2004; 4: 202S–208S.
 46. Wen H, Morris KR and Park K. Hydrogen bonding interactions between adsorbed polymer molecules and crystal surface of acetaminophen. *J Colloid Interface Sci* 2005; 290: 325–335.

47. Kang TW, Han J, Lee S, et al. 2D transition metal dichalcogenides with glucan multivalency for antibody-free pathogen recognition. *Nat Commun* 2018; 9: 2549.
48. Kamali A, Ziadlou R, Lang G, et al. Small molecule-based treatment approaches for intervertebral disc degeneration: current options and future directions. *Theranostics* 2021; 11: 27–47.
49. Recuerda M, Cote SP, Villemure I, et al. Influence of experimental protocols on the mechanical properties of the intervertebral disc in unconfined compression. *J Biomech Eng* 2011; 133: 071006.
50. Frith JE, Cameron AR, Menzies DJ, et al. An injectable hydrogel incorporating mesenchymal precursor cells and pentosan polysulphate for intervertebral disc regeneration. *Biomaterials* 2013; 34: 9430–9440.
51. Thomas JD, Fussell G, Sarkar S, et al. Synthesis and recovery characteristics of branched and grafted PNIPAAm-PEG hydrogels for the development of an injectable load-bearing nucleus pulposus replacement. *Acta Biomater* 2010; 6: 1319–1328.
52. Huebsch N, Arany PR, Mao AS, et al. Harnessing traction-mediated manipulation of the cell/matrix interface to control stem-cell fate. *Nat Mater* 2010; 9: 518–526.
53. Guilak F, Cohen DM, Estes BT, et al. Control of stem cell fate by physical interactions with the extracellular matrix. *Cell Stem Cell* 2009; 5: 17–26.
54. Zhang GZ, Liu MQ, Chen HW, et al. NF-kappaB signalling pathways in nucleus pulposus cell function and intervertebral disc degeneration. *Cell Prolif* 2021; 54: e13057.
55. Chen F, Jiang G, Liu H, et al. Melatonin alleviates intervertebral disc degeneration by disrupting the IL-1beta/NF-kappaB-NLRP3 inflammasome positive feedback loop. *Bone Res* 2020; 8: 10.
56. Aleissa MS, Alkahtani S, Abd Eldaim MA, et al. Fucoidan ameliorates oxidative stress, inflammation, DNA damage, and hepatorenal injuries in diabetic rats intoxicated with aflatoxin B(1). *Oxid Med Cell Longev* 2020; 2020: 9316751.
57. Matsumoto S, Nagaoka M, Hara T, et al. Fucoidan derived from *Cladosiphon okamuranus* Tokida ameliorates murine chronic colitis through the down-regulation of interleukin-6 production on colonic epithelial cells. *Clin Exp Immunol* 2004; 136: 432–439.
58. Risbud MV and Shapiro IM. Role of cytokines in intervertebral disc degeneration: pain and disc content. *Nat Rev Rheumatol* 2014; 10: 44–56.
59. Li L, Wei K, Ding Y, et al. M2a macrophage-secreted CHI3L1 promotes extracellular matrix metabolic imbalances via activation of IL-13Ralpha2/MAPK pathway in rat intervertebral disc degeneration. *Front Immunol* 2021; 12: 666361.
60. Zhang H, Cai D and Bai X. Macrophages regulate the progression of osteoarthritis. *Osteoarthritis Cartilage* 2020; 28: 555–561.
61. Vincent K, Mohanty S, Pinelli R, et al. Aging of mouse intervertebral disc and association with back pain. *Bone* 2019; 123: 246–259.
62. Tang G, Zhou B, Li F, et al. Advances of naturally derived and synthetic hydrogels for intervertebral disk regeneration. *Front Bioeng Biotechnol* 2020; 8: 745.